

Prevention of tuberculosis in rhesus macaques by a cytomegalovirus-based vaccine

Scott G Hansen^{1,8}, Daniel E Zak^{2,8}, Guangwu Xu^{1,8}, Julia C Ford¹, Emily E Marshall¹, Daniel Malouli¹, Roxanne M Gilbride¹, Colette M Hughes¹, Abigail B Ventura¹, Emily Ainslie¹, Kurt T Randall¹, Andrea N Selseth¹, Parker Rundstrom¹, Lauren Herlache¹, Matthew S Lewis¹, Haesun Park¹, Shannon L Planer¹, John M Turner¹, Miranda Fischer¹, Christina Armstrong¹, Robert C Zweig¹, Joseph Valvo², Jackie M Braun², Smitha Shankar², Lenette Lu³, Andrew W Sylwester¹, Alfred W Legasse¹, Martin Messerle⁴, Michael A Jarvis⁵, Lynn M Amon², Alan Aderem², Galit Alter³, Dominick J Laddy⁶, Michele Stone⁶, Aurelio Bonavia⁶, Thomas G Evans⁶, Michael K Axthelm¹, Klaus Früh¹, Paul T Edlefsen⁷ & Louis J Picker¹

Despite widespread use of the bacille Calmette–Guérin (BCG) vaccine, tuberculosis (TB) remains a leading cause of global mortality from a single infectious agent (*Mycobacterium tuberculosis* or Mtb). Here, over two independent Mtb challenge studies, we demonstrate that subcutaneous vaccination of rhesus macaques (RMs) with rhesus cytomegalovirus vectors encoding Mtb antigen inserts (hereafter referred to as RhCMV/TB)—which elicit and maintain highly effector-differentiated, circulating and tissue-resident Mtb-specific CD4⁺ and CD8⁺ memory T cell responses—can reduce the overall (pulmonary and extrapulmonary) extent of Mtb infection and disease by 68%, as compared to that in unvaccinated controls, after intrabronchial challenge with the Erdman strain of Mtb at ~1 year after the first vaccination. Fourteen of 34 RhCMV/TB-vaccinated RMs (41%) across both studies showed no TB disease by computed tomography scans or at necropsy after challenge (as compared to 0 of 17 unvaccinated controls), and ten of these RMs were Mtb-culture-negative for all tissues, an exceptional long-term vaccine effect in the RM challenge model with the Erdman strain of Mtb. These results suggest that complete vaccine-mediated immune control of highly pathogenic Mtb is possible if immune effector responses can intercept Mtb infection at its earliest stages.

The natural immune response to Mtb infection, characterized pathologically by necrotizing granulomatous inflammation, limits the progression of infection in most subjects, but at the same time it provides a haven for pathogen persistence and promotes host-to-host transmission^{1–4}. An emerging consensus in the field suggests that over many thousands of years of evolution as an obligate human pathogen, Mtb has developed the ability to manipulate the human immune response to achieve the optimal balance between pathogenicity and immunity that provides maximal penetrance in the human population^{1,2,5–7}. Natural Mtb immunity would therefore include a mixture of protective and antiprotective components, the latter of which would contribute to Mtb persistence and transmission. In keeping with this hypothesis, the BCG vaccine, which is derived from *Mycobacterium bovis* and enhances natural adaptive antimycobacterial immunity, is not completely efficacious. BCG protects vaccinated individuals, particularly children, from severe miliary TB, but it fails to substantially reduce the incidence of pulmonary TB in

adolescents and adults, a requirement for vaccine-mediated control of the global TB epidemic^{4,8,9}. A corollary of this hypothesis is that for a vaccine to have sufficient potency to prevent pulmonary TB and thereby have an effect on the TB epidemic, it will likely need to possess the following characteristics: (i) the ability to elicit effective, durable anti-Mtb immune responses that lack the components of natural Mtb immunity that are advantageous to the microbe, and (ii) the ability to control or eliminate any nascent Mtb infection before the microbe's establishment of an immune environment conducive to persistence (which likely includes mature granulomas) and/or be potent enough to overcome any Mtb-associated immunoregulation that contributes to persistence. Studies in the mouse model of TB have shown that accelerating effector cell production and delivery to the lungs in primary Mtb infection improves outcome¹⁰. Consistent with this concept of improved Mtb control with earlier effector cell delivery, vaccination of nonhuman primates (NHPs) via aerosol delivery of either BCG or an attenuated Mtb vaccine strain, which potentiates both innate and

¹Vaccine and Gene Therapy Institute and Oregon National Primate Research Center (ONPRC), Oregon Health and Science University (OHSU), Beaverton, Oregon, USA. ²Center for Infectious Disease Research, Seattle, Washington, USA. ³Ragon Institute of Massachusetts General Hospital, Massachusetts Institute of Technology and Harvard University, Cambridge, Massachusetts, USA. ⁴Department of Virology, Hannover Medical School, Hannover, Germany. ⁵School of Biomedical and Healthcare Sciences, University of Plymouth, Devon, UK. ⁶Aeras, Rockville, Maryland, USA. ⁷Statistical Center for HIV–AIDS Research and Prevention, Vaccine and Infectious Disease Division, Fred Hutchinson Cancer Research Center, Seattle, Washington, USA. ⁸These authors contributed equally to this work. Correspondence should be addressed to L.J.P. (pickerl@ohsu.edu).

Received 1 September 2017; accepted 15 December 2017; published online 15 January 2018; doi:10.1038/nm.4473

adaptive cellular immune responses in the lung, has been shown to enhance protection against Mtb challenge^{11–13}. Heterologous viral vaccine vectors would presumably have advantages over mycobacteria-based vaccines, as these agents would likely lack the antiprotective immunoregulatory manipulation of mycobacteria, yet would potentially have an ability to elicit Mtb-specific CD4⁺ and CD8⁺ T cell responses with relevant functional profiles (for example, the ability to synthesize effector cytokines such as interferon (IFN)- γ and tumor necrosis factor (TNF), which are associated with Mtb control^{1,2,9}). To date, however, TB vaccines based on poxvirus and adenovirus vectors have shown only modest enhancement of Mtb control in NHP models, and a phase 2b trial of a modified vaccinia Ankara/Ag85A vaccine has failed to show clinical benefit^{14–18}.

The reason for the limited success of the poxvirus-based and adenovirus-based vectors as TB vaccines is unknown, but we hypothesize that these particular viral vectors simply failed to elicit, maintain and/or deliver sufficient numbers of functionally appropriate, effector-differentiated Mtb-specific T cells at relevant tissue sites, such as the bronchial mucosa, alveolar tissue and lung-draining lymph nodes (LNs), to effectively control Mtb challenge. In this regard, we and others have previously shown that cytomegalovirus (CMV) is unique among microbial agents that infect humans and NHPs in its ability to elicit and maintain robust, life-long, circulating and tissue-resident, effector-differentiated CD4⁺ and CD8⁺ memory T cell responses^{19,20}. Indeed, CMV-specific CD4⁺ and CD8⁺ T cells constitute an average of 10% of the entire circulating memory T cell population in CMV-infected people²¹. We also have previously demonstrated that RhCMV-based vectors can be exploited as a uniquely effective ‘effector memory’ vaccine against simian immunodeficiency virus (SIV) in RMs^{22–24} and have established that these vectors can elicit and maintain circulating and tissue-resident CD4⁺ and CD8⁺ effector-differentiated T cells (transitional effector memory T (T_{TEM}) cells and fully differentiated effector memory T (T_{EM}) cells) to any exogenous antigen (Ag) insert^{22–25}, including those encoding Mtb proteins²⁵. Because RhCMV-vector-elicited T_{TEM} and T_{EM} cells both circulate in blood and accumulate in the lung, and can produce copious amounts of TNF and IFN- γ after Ag recognition^{22–24}, the RhCMV/TB vaccine provides a unique opportunity to experimentally test the hypothesis that such high-frequency, preformed, *in situ* or rapidly recruited, Mtb-specific TNF- and IFN- γ -producing T_{TEM} and T_{EM} cells would be able to abrogate or markedly reduce TB progression after highly pathogenic Mtb challenge.

RESULTS

Relative immunogenicity of RhCMV/TB and BCG (Study 1)

RMs are highly susceptible to Mtb infection (particularly the highly pathogenic Erdman strain), even at very low doses of challenge inoculum, and show immunological and pathological responses that are very similar to those seen in humans, except that, whereas most (~85–90%) human TB infections are nonprogressive over the lifetime of the infected individual, the vast majority of Mtb-infected RMs progress to disease following experimental exposure^{4,26–30}. Mtb infection of RMs therefore represents a close-to-human, yet extremely stringent, model for testing TB vaccine activity. Indeed, the protection afforded by intradermally (i.d.) administered BCG vaccine in this model is variable and modest^{8,13,16,31}, allowing vaccine developers to target enhancement of protection over that of i.d. administered BCG in this model as the goal of any new TB vaccine concept.

To test the hypothesis that vaccination with a RhCMV/TB vaccine would elicit more effective immunity than i.d. administered BCG

and/or enhance the protection of i.d. administered BCG, we vaccinated three groups of RMs ($n = 7$ /group; all of which were naturally RhCMV⁺ at study assignment) with the following vaccines: (i) RhCMV/TB alone (subcutaneous administration of a set of four RhCMV vectors based on the 68-1 RhCMV strain that together expressed nine different Mtb proteins: ESAT-6, Ag85A, Ag85B, Rv3407, Rv1733, Rv2626, Rpf A, Rpf C and Rpf D; **Supplementary Fig. 1a**), (ii) i.d. administered BCG alone or (iii) i.d. administered BCG followed (6 weeks later) by subcutaneous vaccination with RhCMV/TB (**Fig. 1a**). As expected, the RhCMV/TB vaccine elicited and maintained a high frequency of CD4⁺ and CD8⁺ T cell responses in blood to all nine Mtb inserts, as measured by overlapping 15-mer peptide mix-induced expression of intracellular TNF and/or IFN- γ by flow cytometric intracellular cytokine (ICS) analysis (**Fig. 1b,c**). During the plateau phase, RhCMV-vector-elicited Ag85A-specific responses were predominantly effector-differentiated, manifesting an almost exclusive T_{EM} phenotype for CD8⁺ T cell responses, and a mixed T_{TEM} and T_{EM} phenotype for CD4⁺ T cell responses (**Fig. 1d**). Approximately half of the RhCMV/TB-elicited Ag85A-specific CD4⁺ and CD8⁺ T cells responding in the ICS assays produced both TNF and IFN- γ (with or without interleukin (IL)-2), with the remainder predominantly producing TNF alone (**Fig. 1e**). BCG induced circulating CD4⁺ and CD8⁺ T cell responses to eight of the nine expressed Ags (all except ESAT-6, which is not expressed by BCG³²). In peripheral blood, the overall magnitude of the BCG-elicited T cell responses to these eight Ags was considerably less than that observed in RhCMV/TB-vaccinated RMs (**Fig. 1b,c**). BCG-elicited Ag85A-specific responses predominantly showed a central memory (T_{CM}) cell phenotype for the CD4⁺ T cells, and a T_{EM} cell phenotype for the CD8⁺ T cells (**Fig. 1d**). The majority of these Ag85A-specific T cells produced either TNF or IL-2 alone (CD4⁺), or TNF or IFN- γ alone (CD8⁺), but not both TNF and IFN- γ (**Fig. 1e**). Notably, the BCG-induced CD4⁺ and CD8⁺ T cell response to the eight BCG-expressed Mtb Ags was not large enough to significantly change the plateau-phase magnitude, phenotype or function of the peripheral blood Mtb-Ag-specific responses in the RMs that were administered both BCG and RhCMV/TB, relative to that in the RMs that received the RhCMV/TB vaccine alone (**Fig. 1b–e**). Differences in the magnitude of the responses between the BCG- and RhCMV/TB-vaccinated RMs were less apparent in bronchoalveolar lavage (BAL) fluid, with the responses in the latter group being only modestly higher than that in the former group (**Fig. 1f**). None of the three types of vaccinations used in Study 1 elicited significant antibody (Ab) responses to the nine TB Ags in the RhCMV vector inserts (**Supplementary Fig. 1b**).

Effect of BCG, RhCMV/TB and BCG + RhCMV/TB vaccination on Mtb challenge (Study 1)

Fifty weeks after the initial BCG vaccination, the three groups of vaccinated RMs and a control group of unvaccinated RMs ($n = 8$; all of which were naturally RhCMV⁺) were challenged by intrabronchial instillation of 25 colony-forming units (CFUs) of Erdman strain Mtb bacteria into the right lower lobe. The effectiveness of challenge was confirmed by *de novo* development of CD4⁺ and CD8⁺ T cell responses to the CFP-10 Ag (**Fig. 2a** and **Supplementary Fig. 2a**; note that the Mtb-expressed CFP-10 Ag was not included in the RhCMV/TB vectors, and, like ESAT-6, it is not expressed by BCG³²). The unvaccinated RMs manifested *de novo* CD4⁺ and CD8⁺ T cell responses to all nine TB-vaccine-insert Ags, including strong responses to ESAT-6 (**Fig. 2b** and **Supplementary Fig. 2b**). Only very modest increases in the magnitude of CD4⁺ and CD8⁺ T cell responses to the

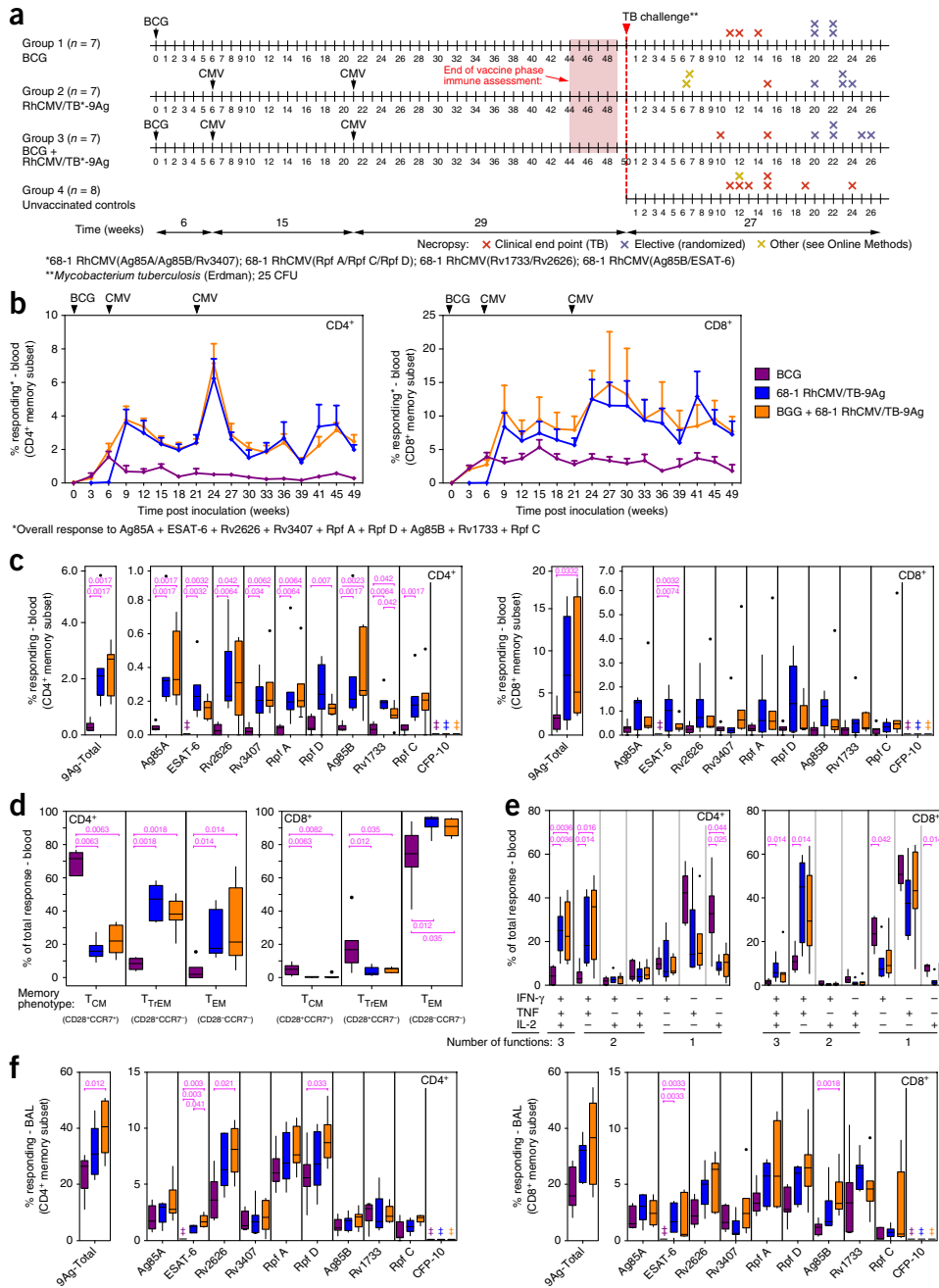


Figure 1 Immunogenicity of RhCMV/TB and i.d. administered BCG vaccines (Study 1). **(a)** Schematic of the RM groups ($n = 29$ biologically independent animals), vaccination and challenge protocols, and necropsy time points in Study 1. **(b)** Longitudinal analysis of the overall CD4⁺ and CD8⁺ T cell response to the nine Mtb proteins expressed after vaccination. The background-subtracted frequencies of cells that produced TNF and/or IFN- γ by a flow cytometric ICS assay to peptide mixes comprising each of the Mtb proteins within the memory CD4⁺ or CD8⁺ T cell subsets were totaled, with the figure showing the mean (+ s.e.m.; $n = 7$ per group) of these overall (total) responses at each time point. **(c)** Box plots comparing the individual Mtb-protein-specific (for each of the nine Mtb inserts plus the non-insert CFP-10) and overall (total) Mtb-specific CD4⁺ and CD8⁺ T cell response frequencies (as defined by TNF and/or IFN- γ production) in peripheral blood between the same vaccine groups as in **b**, at the end of the vaccine phase (each data point is the mean of response frequencies in three separate samples from weeks 44–49). **(d)** Box plots comparing memory differentiation of the vaccine-elicited CD4⁺ and CD8⁺ memory T cells in peripheral blood in response to Ag85A, with TNF and/or IFN- γ production at the end of vaccine phase (week 47). Memory differentiation state was based on CD28 versus CCR7 expression, which delineated between central memory (T_{CM}), transitional effector memory (T_{TREM}) and effector memory (T_{EM}) cells, as designated. **(e)** Box plots comparing the frequency of vaccine-elicited CD4⁺ and CD8⁺ memory T cells in peripheral blood in response to Ag85A, with TNF, IFN- γ and IL-2 production, alone or in all combinations, at the end of vaccine phase (week 49). **(f)** Box plots comparing the individual Mtb-protein-specific and overall (total) Mtb-specific CD4⁺ and CD8⁺ T cell frequencies (as defined by TNF and/or IFN- γ production) in bronchoalveolar lavage (BAL) fluid between the vaccine groups at the end of the vaccine phase (weeks 46–47). In **c–f**, plots show a box from first to third quartiles (IQR) and a line at the median, with whiskers extending to the farthest data point within $1.5 \times$ the interquartile range (IQR) above and below the box respectively; all data points outside of the whiskers are plotted individually. The Kruskal–Wallis (KW) test was used to determine the significance of differences between vaccine groups, and the Wilcoxon rank-sum test was used to perform pair-wise analysis for KW P values that were ≤ 0.05 ; brackets indicate pair-wise comparisons with Holm-adjusted, two-sided Wilcoxon $P \leq 0.05$ values shown ($n = 7$ per group). The double dagger symbol (§) indicates that no response was detected.

TB-vaccine-insert Ags were detected after Mtb challenge in vaccinated RMs from all three vaccine groups (shown as the percentage change in response from baseline; **Fig. 2b** and **Supplementary Fig. 2b**).

The observation that the magnitude of this change from baseline after challenge in the vaccinated RMs was not significantly different from the magnitude of the *de novo* responses to challenge in unvaccinated

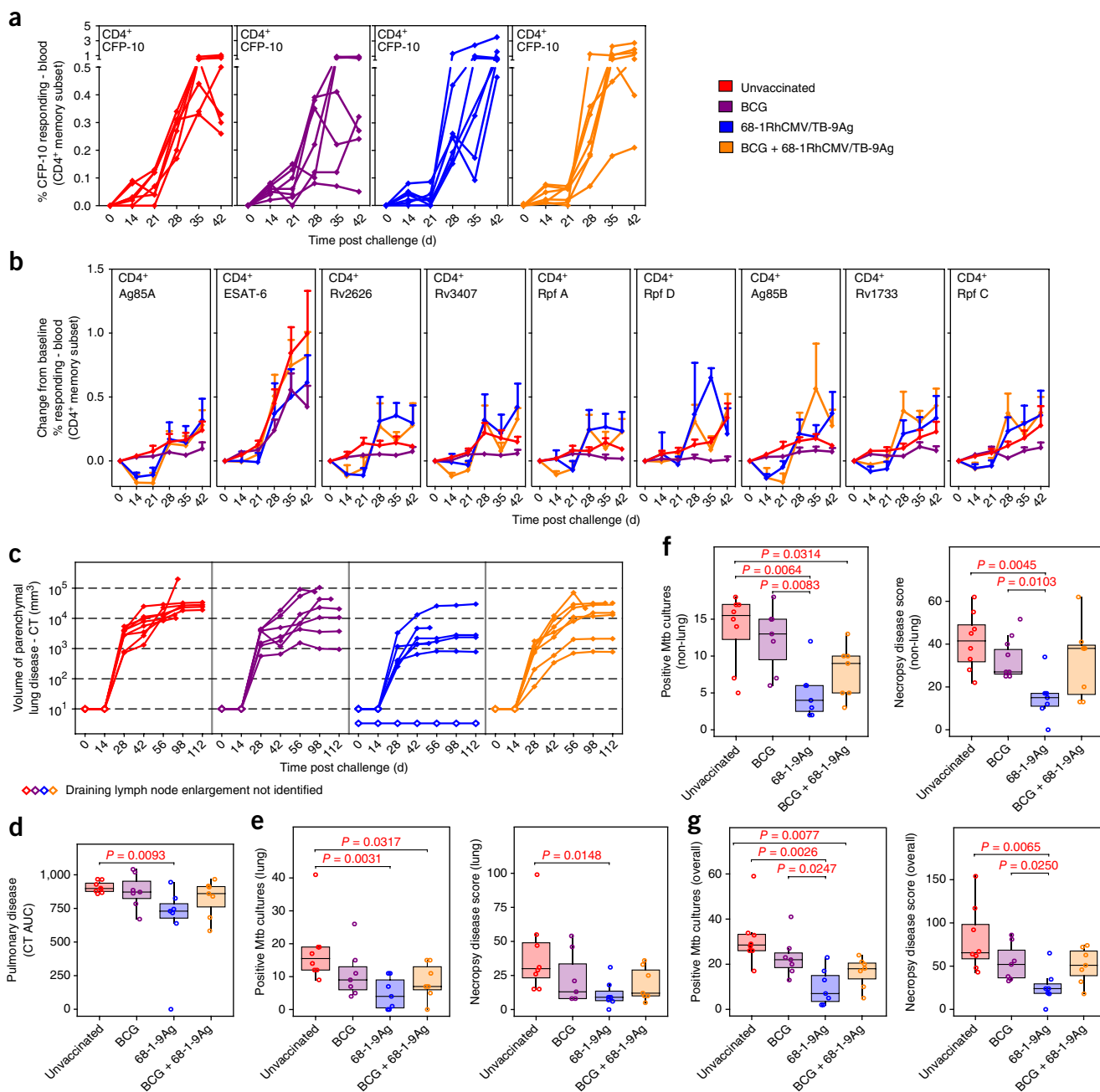


Figure 2 Outcome of Mtb challenge (Study 1). **(a)** Peripheral blood CD4⁺ T cell responses to peptide mixes comprising the Mtb protein CFP-10 (not expressed by the study vaccines), after Mtb challenge, as assessed by flow cytometric ICS analysis (response defined by TNF and/or IFN- γ production after background subtraction in memory subset; CFP-10-specific CD8⁺ T cell responses shown in **Supplementary Fig. 2a**; $n = 7$ RMs per vaccine group; $n = 6$ unvaccinated RMs). **(b)** Mean (\pm s.e.m.; $n = 7$ per group; $n = 6$ unvaccinated RMs) change in peripheral blood CD4⁺ T cell response frequencies specific for the indicated vaccine-expressed Mtb proteins after Mtb challenge relative to pre-challenge baseline value, as assessed by flow cytometric ICS analysis (response defined as in **a**; analogous CD8⁺ T cell responses shown in **Supplementary Fig. 2b**). There were no significant differences in the response dynamics (post-challenge change in value relative to that in baseline) between unvaccinated RMs and any of the vaccine groups (Online Methods). **(c)** Quantification of disease volume, as assessed using CT scans, in the pulmonary parenchyma after Mtb challenge (presence or absence of draining LN enlargement indicated by closed versus open symbols). **(d)** Box plots comparing the AUC of CT-determined pulmonary lesional volume (day 0–112; Online Methods) of the four RM groups. **(e–g)** Box plots comparing the extent of TB at necropsy, as measured by Mtb recovery with mycobacterial culture and by pathologic disease score (Online Methods), in lung parenchyma **(e)**, all non-lung parenchymal tissues **(f)** and all tissues **(g)**. In **c–g**, $n = 7$ per vaccine group and $n = 8$ unvaccinated RM; in **d–g** plots show jittered points with a box from first to third quartiles (IQR) and a line at the median, with whiskers extending to the farthest data point within $1.5 \times$ IQR above and below the box respectively. Unadjusted $P \leq 0.05$ values by two-sided Wilcoxon test are shown (see also **Supplementary Fig. 4a**).

RMs suggested that none of the vaccines used in this study were able to prime for an anamnestic Mtb-specific T cell response (i.e., a secondary, systemic immune response of substantially greater magnitude than the primary response). Initially, we planned to monitor post-challenge pulmonary immune responses by BAL fluid analysis; however, BAL was discontinued after two RMs were euthanized and taken to necropsy due to acute cardiopulmonary complications associated with the BAL procedure (Online Methods). The development of pulmonary disease after challenge was monitored every 2 weeks by computed tomography (CT)-based assessment of lesion volume, and both pulmonary and extrapulmonary disease were determined at necropsy, with necropsy targeted to be performed either at the clinical end point or after 20 weeks post infection (p.i.), by randomization (Fig. 1a). The extent of Mtb infection and TB disease at necropsy was quantified by: (i) detailed pathologic scoring (on the basis of comprehensive gross and microscopic pathological examinations; see Supplementary Fig. 3 and Online Methods), (ii) the frequency of recovery of culturable Mtb from a standard set of tissue samples, including 40 lung-punch biopsies (randomly sampled using stereology to standardize sample collection across all of the RMs in the study), as well as representative samples of trachea, all lung-draining and other chest LNs (hilar, carinal, paratracheal and mediastinal), selected peripheral LNs (axillary, inguinal and mesenteric) and other selected organs (spleen, liver, kidney and pancreas), and (iii) the amount of culturable Mtb in lung-draining LNs (CFU per g tissue), a nearly universal site of Mtb infection in RMs with progressive TB disease²⁶.

Pulmonary disease developed rapidly in unvaccinated control RMs, with progression to severe ($\geq 10,000$ mm³ of total lesional volume) lung parenchymal disease, as determined by CT scans, in seven of eight RMs by day 56 p.i. and in all RMs by day 98 p.i. (Fig. 2c). In both of the RM groups that received i.d. administered BCG, the development of pulmonary disease was more variable; however, five of seven RMs in each group developed severe disease by day 98 p.i. In contrast, five of the seven RMs that were vaccinated with RhCMV/TB alone developed only mild pulmonary disease ($< 3,000$ mm³ of total lesional volume; $n = 4$) or no disease ($n = 1$). The overall area-under-the-curve (AUC) value of pulmonary lesion volume of the 'RhCMV/TB alone' group during the first 16 weeks p.i. (using imputed AUC values for monkeys taken to necropsy before week 16 p.i.; Online Methods) was significantly reduced as compared to that for the unvaccinated control group (Fig. 2d and Supplementary Fig. 4a), whereas there was no significant reduction in this parameter in the groups administered BCG alone or BCG + RhCMV/TB. Across all groups, the CT-determined lesional AUC through week 16 closely correlated with pulmonary parenchymal disease at necropsy, as measured by both pathologic scoring and extent of Mtb recovery by culture (Supplementary Fig. 5a), and consistent with this, the extent of pulmonary TB at necropsy was also significantly reduced in the RhCMV/TB group as compared to that in the unvaccinated controls by both of these necropsy measures (Fig. 2e and Supplementary Fig. 4a). No significant reduction in pulmonary disease was observed in the BCG-only vaccinated cohort by either necropsy measure, and the regimen with vaccine combination of BCG + RhCMV/TB resulted in a significant reduction in Mtb burden, but not in pathologic score (Fig. 2e and Supplementary Fig. 4a).

TB is typically not restricted to pulmonary parenchyma in RMs infected with the Erdman strain of Mtb²⁶, and necropsy analysis revealed extensive extrapulmonary disease in the unvaccinated RMs, including both lung-associated LN involvement and extrathoracic spread (Supplementary Fig. 6). Notably, the extent of overall disease,

as measured by the pathologic score, also closely correlated with the recovery of viable Mtb in pulmonary and nonpulmonary parenchymal tissues (Supplementary Fig. 5b), and by both the pathologic score and Mtb-recovery criteria, extrapulmonary and overall disease were significantly reduced in the RhCMV/TB-vaccinated cohort relative to that in the unvaccinated RMs (Fig. 2f,g and Supplementary Fig. 4a). We also found a > 2 -log reduction in the density of culturable Mtb (CFU/g) in all lung-draining LNs in RhCMV/TB-vaccinated RMs as compared to that in unvaccinated control RMs ($P = 0.0003$; Supplementary Fig. 5e). By Poisson modeling, the overall (pulmonary + extrapulmonary) extent of disease was reduced in the RhCMV/TB-vaccinated group by 68.7%, as determined by extent of Mtb recovery ($P < 0.0001$), and by 67.3%, using the pathologic score ($P < 0.0001$), relative to that in unvaccinated controls (Supplementary Fig. 4b). In contrast, the extent of extrapulmonary and overall disease in BCG-vaccinated RMs was not significantly different from that in unvaccinated RMs by either criterion (Fig. 2f,g and Supplementary Fig. 4a). The density of viable mycobacteria in lung-draining LNs was also not different in BCG-vaccinated RMs relative to that in unvaccinated controls (Supplementary Fig. 5e). Consistent with these results, the extent of extrapulmonary and overall disease, as well as the density of viable Mtb in lung-draining LNs, in RMs that received RhCMV/TB alone were also significantly reduced when directly compared to those in BCG-vaccinated RMs (Fig. 2f,g and Supplementary Figs. 4a and 5e). Using the same Poisson modeling, RhCMV/TB vaccination was found to reduce overall disease, relative to that in RMs vaccinated with BCG alone, by 57.7% ($P = 0.0007$) and 51.4% ($P = 0.01$) for the extent of Mtb recovery and pathologic score, respectively (Supplementary Fig. 4b). Vaccination of RMs with i.d. administered BCG 6 weeks before the initial vaccination with RhCMV/TB seemed to reduce both the pulmonary and extrapulmonary protection mediated by the RhCMV/TB vaccination alone, as the BCG + RhCMV/TB group did not manifest a significant reduction in pathologic score relative to that in the unvaccinated controls (Fig. 2e–g and Supplementary Fig. 4a). However, the extent of Mtb recovery in both pulmonary and extrapulmonary tissues, and the density of viable Mtb in lung-draining LNs, was still significantly reduced in the RMs that received BCG + RhCMV/TB relative to that in the unvaccinated controls (Fig. 2e–g and Supplementary Figs. 4a and 5e). Thus, RhCMV/TB-vaccinated RMs manifested superior overall outcomes as compared to RMs that were vaccinated with BCG alone, and the administration of BCG 6 weeks before the RhCMV/TB vaccination seemed to reduce, but not abolish, the protection afforded by the RhCMV/TB vaccine.

Immunogenicity and protective capacity of RhCMV/TB variants (Study 2)

To confirm and further characterize the protective effect of the RhCMV/TB vaccine, we performed a second larger Mtb challenge study ($n = 9$ /group; all of the RMs were naturally RhCMV⁺ at assignment) in which we compared RMs administered the same 68-1 RhCMV backbone-based nine-antigen-encoding (hereafter referred to as RhCMV/TB-9-Ag) vector set used in Study 1 (group 1) with RMs administered an analogous RhCMV/TB-9-Ag vector set based on the 68-1.2 RhCMV backbone (group 2) or with RMs administered a 68-1 RhCMV/TB-6-Ag vector expressing a single six-antigen Mtb polyprotein (Ag85A, ESAT-6, Rv3407, Rv2626, Rpf A and Rpf D) (group 3) (Fig. 3a and Supplementary Fig. 1a). Strain 68-1 RhCMV vectors elicit unconventional CD8⁺ T cell responses that are restricted by major histocompatibility complex (MHC)-II and MHC-E, whereas the

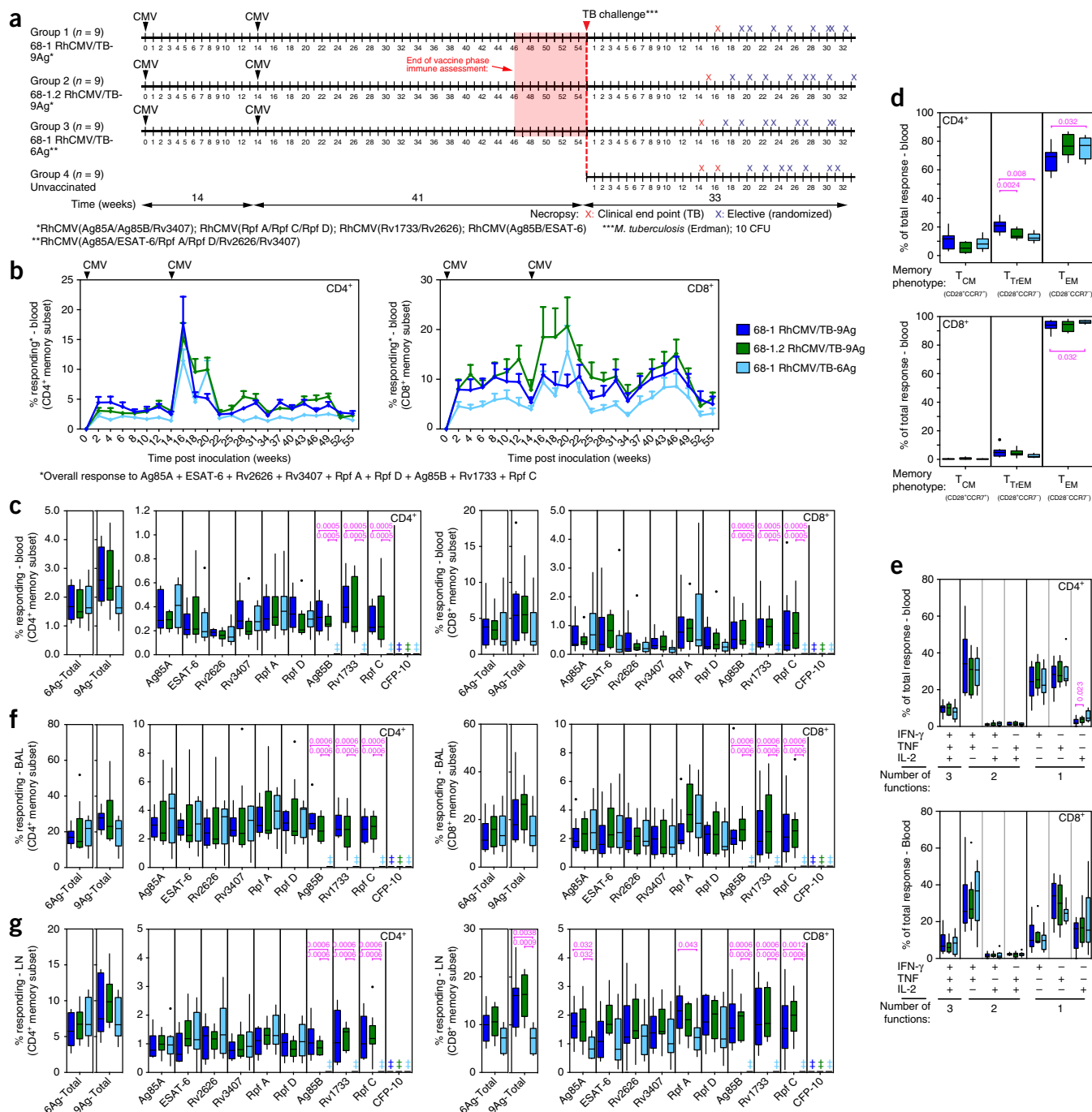


Figure 3 Immunogenicity of RhCMV/TB vaccines (Study 2). **(a)** Schematic of the RM groups, vaccination and challenge protocols, and necropsy time points of Study 2 ($n = 36$ biologically independent animals). **(b)** Longitudinal analysis of the overall CD4⁺ and CD8⁺ T cell response to the nine Mtb Ags after vaccination, as described in **Figure 1b** ($n = 9$ per group). **(c)** Box plots comparing the CD4⁺ and CD8⁺ T cell response frequencies to the individual Mtb proteins (each of the nine Mtb inserts plus the non-insert CFP-10), and the overall (total) Mtb-specific CD4⁺ and CD8⁺ T cell response frequencies (defined by TNF and/or IFN- γ production), in peripheral blood between the vaccine groups at the end of the vaccine phase (each data point is the mean of response frequencies in three separate samples from weeks 49–55). **(d)** Box plots comparing the memory differentiation phenotypes (see **Fig. 1d**) of the vaccine-elicited CD4⁺ and CD8⁺ memory T cells in peripheral blood that respond to Ag85A, with TNF and/or IFN- γ production, at the end of vaccine phase (weeks 51–52). **(e)** Box plots comparing the frequency of vaccine-elicited CD4⁺ and CD8⁺ memory T cells in peripheral blood that respond to Ag85A with TNF, IFN- γ and/or IL-2, alone or in all combinations, at the end of vaccine phase (weeks 49–50). **(f, g)** Box plots comparing Mtb-specific CD4⁺ and CD8⁺ T cell response frequencies to the individual Mtb proteins (the nine Mtb inserts plus the non-insert CFP-10), as well as the overall (summed) Mtb-specific CD4⁺ and CD8⁺ T cell response frequencies (defined by TNF and/or IFN- γ production), in BAL fluid **(f)** and peripheral LNs **(g)** between the vaccine groups at the end of vaccine phase (weeks 46–47). In **c–g**, plots show a box from first to third quartiles (IQR) and a line at the median, with whiskers extending to the farthest data point within $1.5 \times$ IQR above and below the box respectively; all data points outside of the whiskers are plotted individually. Statistical analyses were performed as described in **Figure 1** with brackets indicating pair-wise comparisons with Holm-adjusted, two-sided Wilcoxon $P \leq 0.05$ values (with actual P values shown; $n = 9$ per group). The double dagger symbol (‡) indicates that no response was detected.

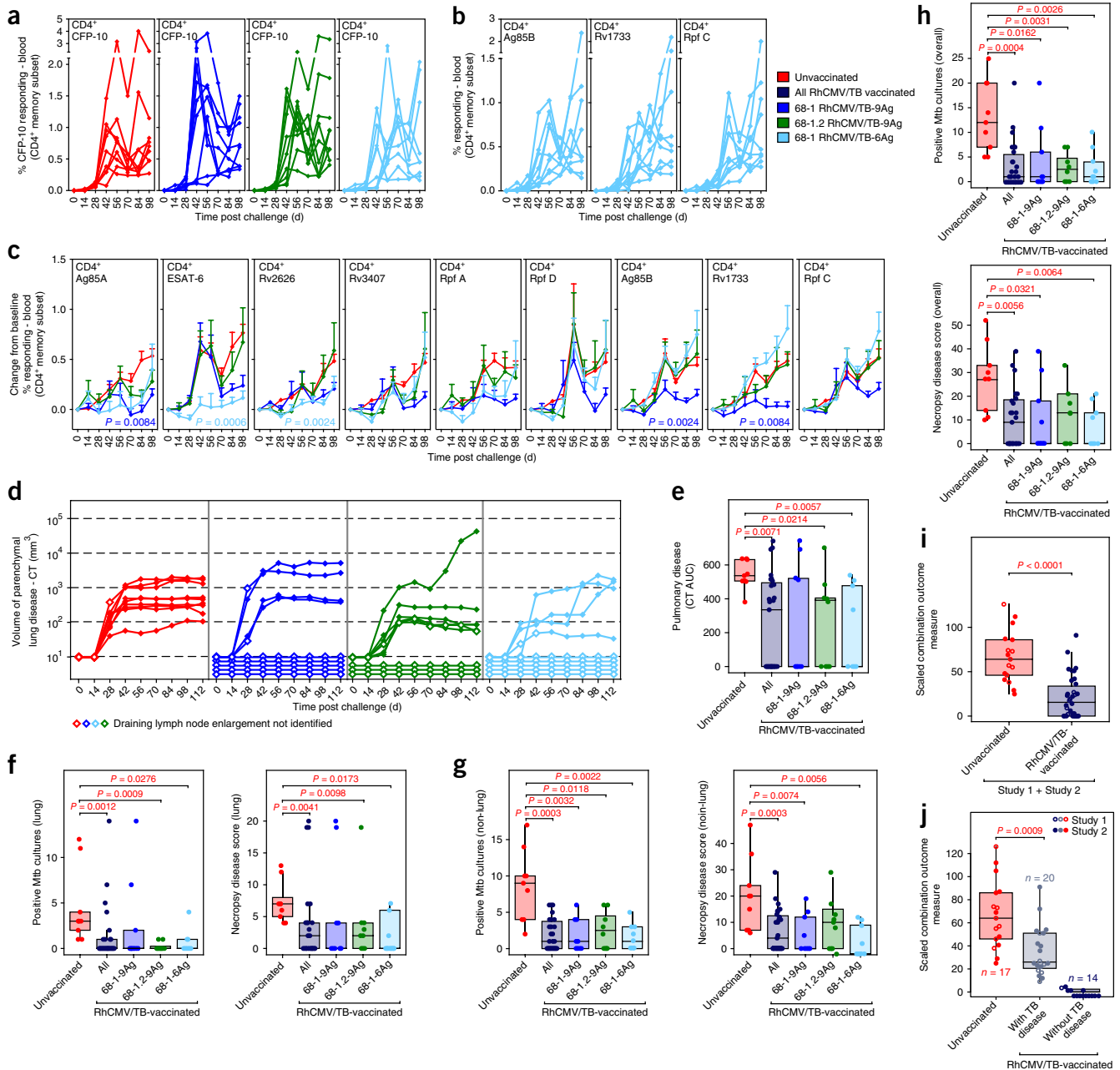


Figure 4 Outcome of Mtb challenge (Study 2 and overall). (**a,b**) Peripheral blood CD4⁺ T cell responses to peptide mixes comprising the Mtb protein CFP-10 in all Study 2 RMs (**a**), or comprising the Ag85B, Rv1733 and Rpf C proteins in group 3 RMs only (RMs vaccinated with the single 68-1 RhCMV/TB-6Ag vector lacking expression of these three proteins) (**b**) after Mtb challenge, as assessed by the flow cytometric ICS analysis described in **Figure 2a** (peripheral blood CD8⁺ T cell responses and tissue CD4⁺ and CD8⁺ T cell responses to these same Ags are shown in **Supplementary Figs. 2c,d and 8**, respectively). (**c**) Mean (+s.e.m.; $n = 9$ per group) change in peripheral blood CD4⁺ T cell response frequencies to peptide mixes comprising the vaccine insert Mtb proteins after Mtb challenge relative to the pre-challenge baseline values, as assessed by the flow cytometric ICS analysis described in **Figure 2b** (analogous CD8⁺ T cell responses are shown in **Supplementary Fig. 2e**). Holm-adjusted Wilcoxon $P \leq 0.05$ are shown for change-from-baseline AUC values of post-challenge responses in any of the vaccinated groups versus those in the unvaccinated controls. (**d**) CT-scan-based quantification of disease volume in the pulmonary parenchyma after Mtb challenge (presence or absence of draining LN enlargement indicated by closed and open symbols, respectively; $n = 9$ per group). (**e**) Box plots comparing the AUC values of CT-scan-determined pulmonary lesion volume (day 0–112) of the unvaccinated RMs versus those in all RhCMV/TB-vaccinated RMs versus RMs in each individual RhCMV/TB vaccine group ($n = 9$ per group). (**f–h**) Box plots comparing the extent of TB at necropsy, as measured by Mtb recovery with mycobacterial culture and by pathologic disease score, in lung parenchyma (**f**), all non-lung parenchymal tissues (**g**) and all tissues (**h**) in the same RM groups as in **e**. (**i,j**) Box plots and unadjusted two-sided Wilcoxon test P values comparing the outcome of Mtb challenge in all unvaccinated RMs versus all RhCMV/TB-vaccinated RMs across both Study 1 ($n = 8$ versus $n = 7$, respectively) and Study 2 ($n = 9$ versus $n = 27$, respectively) using a scaled outcome measure that combines both Mtb culture and pathologic score data (Online Methods) (**i**); in **j**, the RhCMV/TB-vaccinated RMs were divided into two groups on the basis of the presence ($n = 20$) or absence ($n = 14$) of granulomatous disease at necropsy (necropsy pathologic score ≥ 4 versus 0, respectively) versus $n = 17$ unvaccinated RMs. In **e–j**, plots show jittered points with a box from first to third quartiles (IQR) and a line at the median, with whiskers extending to the farthest data point within $1.5 \times$ IQR above and below the box, respectively. Unadjusted, two-sided Wilcoxon $P \leq 0.05$ values are shown (see also **Supplementary Fig. 4**).

Rh157.5/Rh157.4 gene-repaired 68-1.2 RhCMV vectors elicit CD8⁺ T cells that target conventionally MHC-Ia-restricted epitopes^{25,33}. The comparison of group 1 to group 2 therefore allowed determination of the contribution of unconventionally restricted CD8⁺ T cells to RhCMV/TB-mediated protection. In the group 1 versus group 3 comparison, we sought to determine whether the vaccine effect observed in Study 1 with the RhCMV/TB four-vector set encoding nine Mtb Ags (three each in the acute phase, latency and resuscitation Ag types) could be recapitulated by a single RhCMV/TB vector expressing six Mtb Ags (two each from these Ag types) as a single polyprotein, a simpler vaccine configuration which is better suited for clinical translation. As expected, the magnitude of the overall Mtb-specific and individual Mtb-insert-specific CD4⁺ and CD8⁺ T cell responses elicited by the 68-1 and 68-1.2 RhCMV/TB-9-Ag vectors were comparable in blood throughout the vaccination phase, and in the BAL fluid and peripheral LNs at the end of vaccination phase, as was the memory differentiation and functional phenotype of the Mtb-specific response in blood (Fig. 3b–g). However, also as expected²⁵, the CD8⁺ T cells elicited by the 68-1 RhCMV/TB vaccine were unconventionally (MHC-II and MHC-E) restricted, whereas those elicited by the 68-1.2 RhCMV/TB vaccine were conventionally (MHC-Ia) restricted (Supplementary Fig. 7). The T cell responses specific for the six Ags that were common to both the 68-1 RhCMV/TB-6-Ag and RhCMV/TB-9-Ag vaccines were similar between groups 1 and 3 with respect to magnitude, phenotype and (unconventional) MHC restriction, except for slightly different levels of CD8⁺ T cell responses in peripheral LNs (Fig. 3b–g and Supplementary Fig. 7). Thus, the three different RhCMV-based vaccines used in Study 2 generated CD4⁺ and CD8⁺ T cell responses to insert Ags that were of comparable magnitude, function and phenotype, but differed, as intended, in the epitope targeting and restriction of the CD8⁺ T cell responses (68-1 versus 68-1.2), or in the number of Mtb Ags targeted (a six-Ag-encoding single vector versus a nine-Ag-encoding four-vector set). As in Study 1, none of the three RhCMV/TB vaccines used in Study 2 elicited an Ab response specific to any of the TB Ags expressed by these vectors (Supplementary Fig. 1c).

After a 56-week vaccination period, all of the vaccinated RMs (groups 1–3) and unvaccinated control RMs (group 4) were intra-bronchially challenged with ~10 CFUs of Erdman strain Mtb bacteria—the reduction in dose relative to Study 1 was intended to slow TB progression in Study 2 RMs to more closely resemble the course of human Mtb infection. In addition, BAL was not performed after challenge in this experiment to prevent procedure-related mortality and the possibility of artificially enhancing the spread of bacteria within the lung. All Study 2 RMs developed *de novo* CFP-10-specific T cell responses in blood following challenge, and the RMs vaccinated with RhCMV/TB-6-Ag (group 3) also developed *de novo* T cell responses in blood to the Ag85B, Rpf C and Rv1733 Ags, which were not included in their vaccine (Fig. 4a,b and Supplementary Figs. 2c,d and 8). As observed in Study 1, the change in magnitude from baseline of the post-challenge TB-insert-specific CD4⁺ and CD8⁺ T cell responses in RhCMV/TB-vaccinated RMs was less than or equal to the magnitude of the *de novo* responses to these Ags in the unvaccinated RMs, confirming lack of a true anamnestic response in the RhCMV/TB-vaccinated animals (Fig. 4c and Supplementary Fig. 2e). All nine unvaccinated RMs (group 4) developed TB lesions, as seen on CT scans, by day 28 p.i., but as anticipated, the disease progression in this study was slower and reached a lower plateau earlier than in Study 1 (Fig. 4d), and only two unvaccinated (group 4) control RMs developed end point TB disease over the course of observation (Fig. 3a). Remarkably, 13 of the 27 vaccinated RMs (five RMs each

in group 1 and group 3, and three RMs in group 2) did not develop any radiologic signs of pulmonary TB (including no CT-detectable hilar adenopathy) at any time point through to the randomly assigned elective necropsy at >16 weeks p.i., and the average CT-determined lesional AUC value in lung parenchyma of the overall cohort of vaccinated RMs was significantly reduced as compared to that in the unvaccinated group 4 (Fig. 4d,e and Supplementary Fig. 4c).

At necropsy, none of the 13 CT-lesion-negative RMs from vaccine groups 1–3 had any macroscopic granulomatous disease, and 10 of these 13 were culture negative in all tissue samples tested (the remaining three were Mtb⁺ in lung-draining LNs only; Supplementary Figs. 5c,d and 9). Moreover, despite the development of CD4⁺ and CD8⁺ T cell responses to Mtb proteins that were not present within their vaccines in the lung, the lung-draining and peripheral LNs, and the spleen (Supplementary Fig. 8), extensive histopathological analysis of lung and lung-draining LNs from these 13 TB-disease-free RMs showed no microscopic granulomatous inflammation. As in Study 1, the pathologic scores at necropsy (same as Study 1) and the extent of Mtb recovery (same as Study 1, except for expansion of analysis to retropharyngeal, submandibular and iliosacral LNs and in tonsils) were again strongly correlated (Supplementary Fig. 5d). The overall extent of disease by both measures was significantly reduced in the overall (pooled groups 1–3) RhCMV/TB-vaccinated group as compared to that in the unvaccinated control group, with no significant difference in protection observed between individual groups 1, 2 and 3, and similar protection being observed in both pulmonary and extrapulmonary tissues (Fig. 4f–h and Supplementary Figs. 4c and 9). For the pooled vaccinated group, the overall reduction in disease extent relative to that in the unvaccinated control group was 74.5% by Mtb culture ($P = 0.0024$) and 61.4% by pathologic score ($P = 0.0011$), using Poisson modeling (Supplementary Fig. 4d).

To assess the effect of RhCMV/TB vaccination (given alone) on the outcome of an Mtb challenge, relative to no vaccination, across Study 1 and Study 2, we used a scaled (normalized) combination outcome parameter based on both Mtb culture and pathologic score (Online Methods). As shown in Figure 4i, the difference in overall (Study 1 + 2) outcome between unvaccinated and only RhCMV/TB-vaccinated RMs was highly significant and corresponded to a 68% reduction in this combined measure of Mtb infection and disease in the vaccinated RMs by Poisson modeling (Supplementary Fig. 4e). Of note, despite the fact that the average extent of TB progression in the unvaccinated control RMs was quite different in Study 1 and Study 2, the relative reduction in infection and disease associated with RhCMV/TB vaccination was similar for each study (Supplementary Fig. 4). Across both Study 1 and Study 2, 14 of 34 RhCMV/TB-vaccinated RMs (41%; 95% confidence interval (CI): 26–58%) manifested no detectable granulomatous disease at necropsy (versus 0 of 17 unvaccinated controls; $P = 0.0018$), and 10 of these 14 were culture-negative for Mtb (Fig. 4j and Supplementary Figs. 6 and 9). Notably, the extent of disease in the remaining RhCMV/TB (only) vaccinees (for example, excluding the RhCMV/TB-vaccinated RMs with no detectable disease and including only those vaccinated RMs with detectable disease at necropsy; $n = 20$) was still significantly reduced as compared to that in the unvaccinated controls (41.5% reduction by Poisson modeling; Fig. 4j and Supplementary Fig. 4e), indicating that in contrast to the ‘all-or-none’ protection of the RhCMV/SIV vaccine against SIV challenge^{23,24}, the vaccine effect of the RhCMV/TB vaccine included both complete and partial protection. Of note, 32 of the 34 RMs vaccinated with RhCMV/TB alone (94%) manifested an extent of disease at necropsy that was less than the median value in the

unvaccinated controls, and 24 of the 34 vaccinated RMs (71%) manifested an extent of disease at or below the lowest level of disease extent observed in the unvaccinated controls (Fig. 4j).

Innate response to Mtb challenge is modified in RhCMV/TB-protected rhesus macaques

Development of active TB after Mtb infection in humans is associated with profound changes in the expression of genes associated with an immune response and inflammation in whole blood^{34–37}. To determine whether the RMs in our study manifested analogous transcriptional changes after Mtb challenge and whether vaccine-associated protection modified this signature, we performed RNA sequencing (RNA-seq) transcriptome analysis of RNA from whole blood that was collected immediately before and 28 d after Mtb challenge (Fig. 5). We first determined whether genes that were significantly upregulated or downregulated in the blood of patients with active TB as compared to that from controls without active TB disease in two African cohorts³⁷ were similarly regulated in the blood of the unvaccinated RM after challenge. As shown in Figure 5a,b, the unvaccinated control RMs in our study displayed a whole-blood transcriptional response to Mtb infection that was highly congruent with the response in humans, involving similar and robust upregulation and downregulation of a common set of genes in immune-associated modules and pathways. We next tested whether the magnitude of induction of this whole-blood transcriptional signature at 28 d after challenge with Mtb was associated with outcome at necropsy across all Study 1 and Study 2 RMs, as measured by the scaled combination outcome parameter described above. We found that a large number of genes that were highly enriched for the interferon transcriptional module exhibited expression patterns that strongly correlated with extent of disease of the Study 1 and Study 2 RMs at necropsy (Fig. 5c–e). These interferon-response-associated genes included members of a signature associated with progression to active TB disease in humans³⁴, classical antiviral responses (for example, *IRF7*, *IFIH1*, *DDX58* and *RSAD2*) and inflammasome components (*AIM2* and *STAT1*). Notably, this TB-disease-associated transcriptional signature was profoundly reduced in the vast majority of RhCMV/TB-vaccinated RMs with complete Mtb control (e.g., no detectable granulomatous disease at necropsy), indicating that in these RMs, protective vaccine-elicited immune responses countered the spread of Mtb early enough after challenge to ameliorate the potent generalized effect of Mtb infection on innate immune signaling.

Correlates of protection

Given the effector memory nature of RhCMV/TB-vaccine-elicited T cell responses, and the lack of anamnestic T cell or relevant Ab responses, the variable level of protection observed in RhCMV/TB-vaccinated RMs (which ranged from complete to none) would likely reflect a composite integration of the frequency and function of RhCMV/TB-vaccine-elicited T cells, as well as that of innate immune effectors, immediately after challenge, at the local sites of early Mtb replication in lung and lung-draining LNs. Because direct immunological interrogation of all of these sites is not possible, we asked whether analysis of accessible, surrogate sites would provide insight into the immunological differences among RhCMV/TB-vaccinated RMs (with or without i.d. administration of BCG) that determine subsequent control or non-control of Mtb challenge. In this regard, the heterogeneity in outcome among all of the RhCMV/TB-vaccinated RMs in Study 1 and Study 2, as measured by the scaled combination outcome parameter described in Figure 4, was not predicted by the ICS-determined magnitudes of the RhCMV/TB-elicited, TNF- and/or

IFN- γ -defined, CD4⁺ and/or CD8⁺ T cell responses in blood or BAL fluid (or in Study 2 only, peripheral LNs) immediately before challenge (Supplementary Fig. 10a–c). In addition, in Study 2 there were no significant differences in the magnitudes of the AUC values of the post-challenge Mtb-Ag-specific CD4⁺ and CD8⁺ T cell responses between the 13 RhCMV/TB-vaccinated RMs that were completely protected after challenge and the 14 RhCMV/TB-vaccinated RMs with TB disease (Supplementary Fig. 10d,e), except for reduced ESAT-6- and CFP-10-specific CD4⁺ T cell responses in the protected group (which likely reflects the lower antigenic loads of these two related acute-phase Ags in the protected RMs after challenge).

These data suggest that the overall Mtb-specific T cell responses measured in these surrogate sites may not accurately reflect the relevant memory T cell responses in lung tissue and lung-draining LNs and/or that the measured responses are not the only, or not the major, limiting immunological factors that determine outcome. To more globally determine whether other peripheral readouts of the immune and inflammatory state are associated with differential outcomes after Mtb challenge in RhCMV/TB-vaccinated RMs, we analyzed the transcriptomes of whole blood from RMs prior to challenge to identify gene expression associations with the scaled combination outcome measure. This analysis revealed a set of 280 genes with pre-challenge expression profiles that were significantly associated with eventual outcome ($P < 0.05$, false discovery rate (FDR) < 0.33), out of which 258 (92%) (Fig. 6a) exhibited no significant pre-challenge association with outcome for unvaccinated or BCG-vaccinated RMs—suggesting that these signatures were associated with outcome only in the context of RhCMV/TB vaccination. Transcriptional module and pathway enrichment analysis revealed significant ($P < 0.05$, FDR < 0.15) over-representation of neutrophil degranulation and innate immunity functions among the genes that were expressed at higher levels in the RMs that would ultimately be protected ('protection signature'), whereas genes that were expressed at higher levels in RMs that would ultimately develop severe disease ('susceptibility signature') were significantly enriched for the T cell transcriptional module (Fig. 6b,c). Although these enrichment-analysis results raise the possibility that relative abundances of specific leukocyte populations before Mtb challenge would be associated with eventual outcome, no significant associations between outcome and leukocyte population counts were identified. Nevertheless, genes that significantly correlated with neutrophil counts were over-represented within the protection signature, whereas genes that significantly correlated with T cell counts (and to a lesser extent, monocytes) were over-represented within the susceptibility signature (Fig. 6a), consistent with the module and pathway analysis results. Visual inspection of the heat map for the protection and susceptibility signatures (Fig. 6a) suggested that the association with protection was predominantly binary, with strongly protected RMs showing a distinct expression pattern as compared to other RMs. Logistic regression modeling of the data supported this interpretation, with 38/77 (49%) and 70/181 (39%) of protection and susceptibility genes, respectively, demonstrating reasonable potential to discriminate the 14 protected RMs from the remaining RhCMV/TB-vaccinated RMs. Because the BCG + RhCMV/TB-vaccinated group from Study 1 exhibited a trend toward impaired protection as compared to that in the RhCMV/TB-vaccinated group alone (despite having similar RhCMV/TB-elicited T cell responses; Fig. 1b–f), we assessed whether expression of the protection signature was impaired on the day of challenge in Study 1 RMs that were vaccinated with BCG + RhCMV/TB RM as compared to that in the RMs that were vaccinated with RhCMV/TB only (Fig. 6d). This analysis revealed that a subset of protection signature

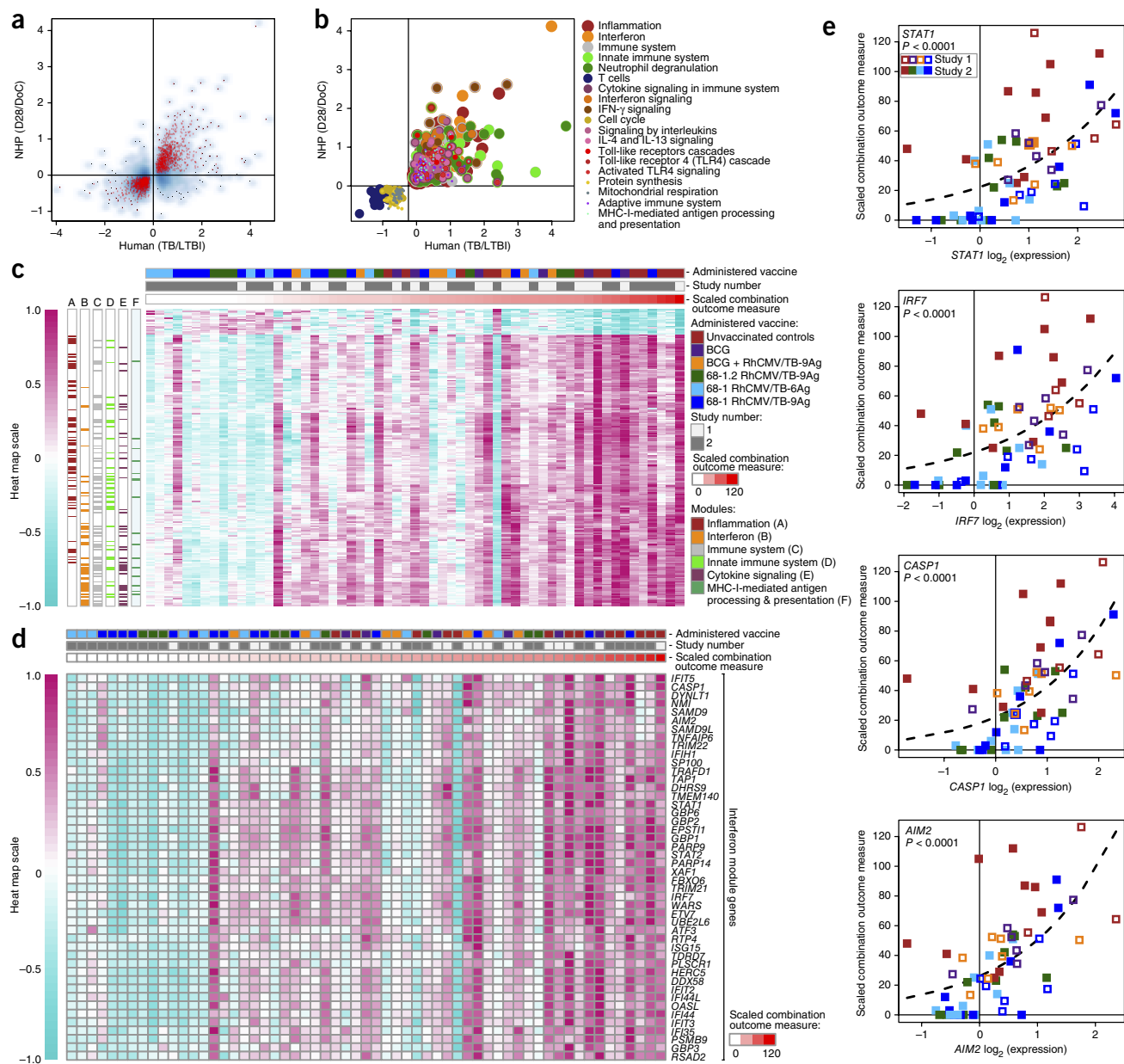


Figure 5 Transcriptional response to Mtb challenge is reduced in protected RMs. **(a)** The median longitudinal \log_2 (fold change in gene expression between day 28 after challenge and the day of challenge) in unvaccinated RMs from Study 1 and Study 2 ($n = 13$; y axis) plotted against the average median \log_2 -transformed expression difference between HIV-negative patients with active TB and control individuals with latent TB infection (LTBI) from South Africa (TB, $n = 46$; LTBI, $n = 48$) and Malawi (TB, $n = 51$; LTBI, $n = 35$) (x axis) for 3,406 significantly regulated genes identified in the human study³⁷. Genes that were significantly regulated in Mtb-challenged, unvaccinated RMs are shown in red (one-sided, paired Wilcoxon rank-sum test, $P < 0.05$; FDR < 0.33 ; complete list of P values shown in **Supplementary Table 1**). The overall Spearman rank correlation coefficient between expression fold changes in the human study and the RMs for all 3,406 genes is 0.58. **(b)** Commonly upregulated ($n = 793$) or downregulated ($n = 689$) genes in humans with TB disease and unvaccinated Study 1 + Study 2 RMs ($n = 13$) 28 d after Mtb infection from **a** were tested for significant over-representation of transcriptional modules⁵³ and immune pathways (Reactome)⁵⁴ ($P < 0.002$ and FDR < 0.01 ; one-sided Fisher's exact test), which were then color-coded according to significance and pathway membership. Enrichment P values ranged from $P < 10^{-40}$ for inflammation and interferon to $P = 2 \times 10^{-3}$ for class I MHC (complete list of P values shown in **Supplementary Table 2**). **(c)** The heat map depicts scaled expression fold changes for all 214 genes for all Study 1 and Study 2 RMs (columns; $n = 59$) ordered by scaled combination outcome measure (red bar at top). Fold changes in post-challenge expression for 214/1,482 commonly regulated genes in **a** were strongly associated with the scaled combination outcome measure as indicated by Poisson modeling ($P < 0.05$ and FDR < 0.1 ; complete list of P values shown in **Supplementary Table 3**). Genes with fold changes that were positively associated with outcome are significantly enriched for the interferon transcriptional module (FDR = 3×10^{-27}) and other pathways (**Supplementary Table 4**). \log_2 (fold changes between day 28 after challenge and day of challenge) values were scaled by the maximum absolute \log_2 (fold change) observed. Annotations of genes to significantly over-represented pathways are shown in colored boxes at the left side of the heat map. **(d)** Heat map, as in **c**, showing expression profiles of 46 genes from the interferon transcriptional module. **(e)** Scatter plots depicting scaled combination outcome measure (y axis) as a function of \log_2 (fold changes between day 28 after challenge and day of challenge) for representative genes from the interferon transcriptional module. The dashed line indicates the best-fit Poisson model. P values indicate the significance of the regression coefficient in a sandwich-adjusted Poisson model ($n = 59$) for the association between gene expression and the scaled combination outcome measure.

genes, including *MMP8*, *CTSG* and *CD52*, were suppressed in the BCG + RhCMV/TB-vaccinated group relative to the RhCMV/TB-vaccinated group, suggesting that BCG-driven modulation of inflammation may

have countered a protective innate immune response in RhCMV/TB-vaccinated RMs, which could thereby have contributed to the reduced protection observed with the combined vaccine regimen.

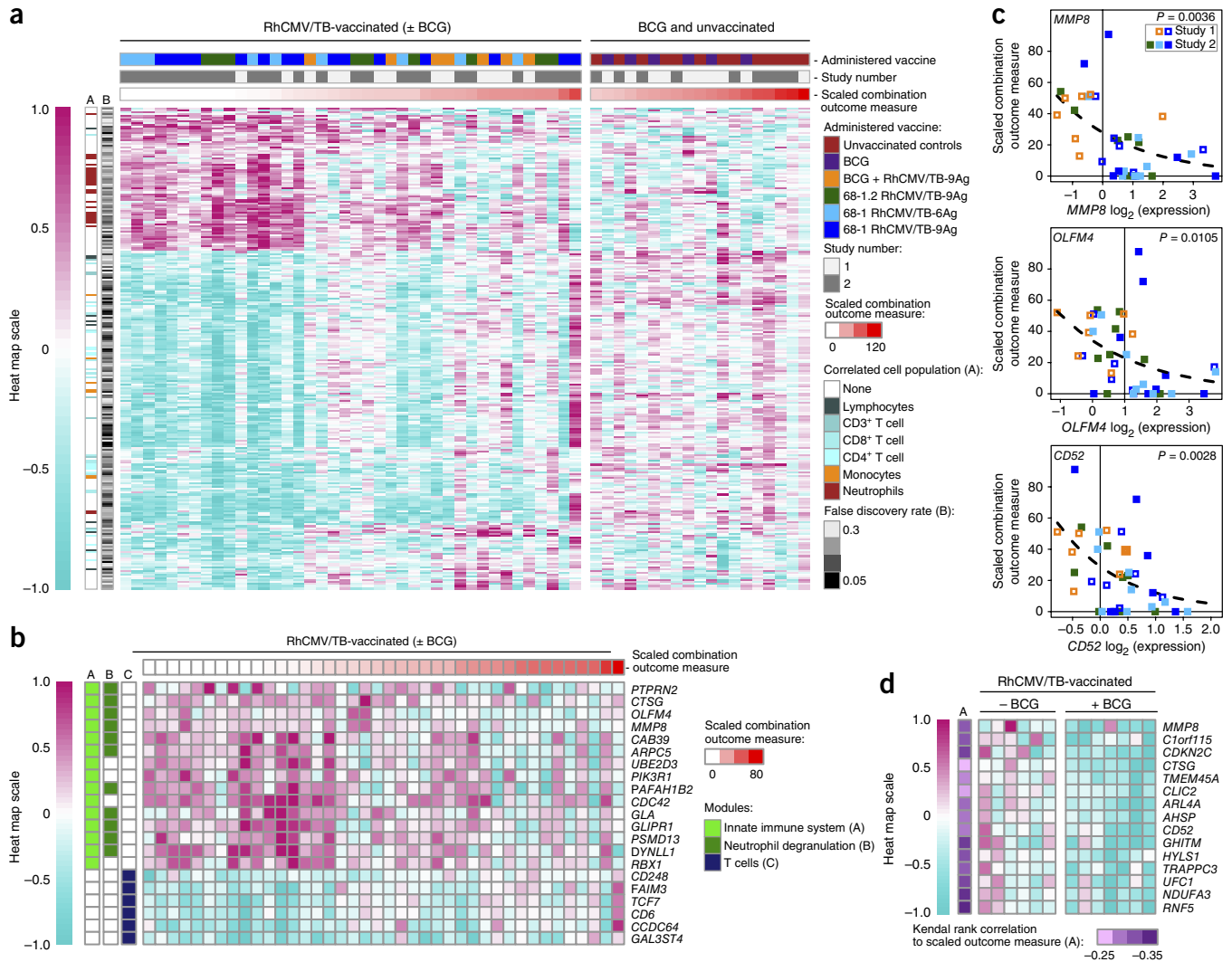


Figure 6 Pre-challenge transcriptional profiles correlate with post-challenge outcome in RhCMV/TB-vaccinated RMs. **(a)** Heat map visualization of the relative gene expression (\log_2 expression fold change) of genes expressed in whole blood immediately before challenge of RhCMV/TB-vaccinated RMs (with or without i.d. administered BCG) from Study 1 + Study 2 that are significantly associated with the scaled combination outcome measure by Poisson modeling ($P < 0.05$ and $FDR < 0.33$; FDR values are shown in the heat map, and all P values are shown in **Supplementary Table 5**; $n = 40$ RMs) and are not associated with outcome for the unvaccinated and BCG-vaccinated RMs ($P > 0.2$; $n = 19$ RM). The left and right sides of the heat map show expression of the genes in RhCMV/TB-vaccinated versus unvaccinated or only-BCG-vaccinated RMs, respectively. The heat map also delineates whether the expression of each gene correlates with the absolute counts of any of the designated leukocyte populations in the same blood sample (if more than one population correlates, then the strongest association is shown; complete results are shown in **Supplementary Table 6**). Note that genes that are positively associated with eventual disease are significantly enriched for genes associated with T cell counts ($FDR < 0.05$; one-sided Fisher's exact test; P values provided in **Supplementary Table 7**), whereas genes that are negatively associated with eventual disease (positively correlated with RhCMV/TB-mediated protection) are significantly enriched for genes associated with neutrophil counts ($FDR = 3 \times 10^{-3}$). **(b)** The testing of genes in **(a)** (protection signature, $n = 77$ genes; susceptibility signature, $n = 181$ genes) for over-representation of transcriptional modules and pathways revealed three significant results ($P < 0.05$, $FDR < 0.15$, one-sided Fisher's exact test), indicated by the colored bars on the left of the heat map (P values provided in **Supplementary Table 8**). The heat map shows the relative expression of specific genes (same scale as in **(a)**) with pre-challenge associations with the scaled combination outcome measure (y axis) as a function of pre-challenge expression of representative protection-associated genes from the neutrophil degranulation module (*MMP8* and *OLF4*, the latter of which is expressed by a neutrophil subset⁵⁵), as well as *CD52*, a broadly expressed gene that is also expressed by neutrophils⁵⁶. The dashed line indicates the best-fit Poisson model (the P values shown indicate the sandwich-adjusted Poisson P values for the association between pre-challenge gene expression and the scaled combination outcome measure; $n = 40$ RM). **(d)** Heat map visualization of 15 genes from **(a)** with protection-associated pre-challenge expression levels that exhibit significantly reduced expression on the day of challenge (one-sided Wilcoxon tests $P < 0.05$ and $FDR < 0.33$) in RMs that were vaccinated with BCG before being vaccinated with RhCMV/TB ($n = 7$), as compared to RMs that were vaccinated with RhCMV/TB only ($n = 6$) in Study 1. See Online Methods for details of data preparation for visualization.

DISCUSSION

Here we demonstrate that subcutaneously administered RhCMV-based TB vaccines are able to elicit and maintain immune effector responses that can control Mtb at the earliest stages of infection and that the protection afforded by this vaccine can be complete, if not sterilizing. To our knowledge, this is the first demonstration of complete prevention of TB disease in a substantial fraction of RMs by a peripherally administered, long-acting vaccine after challenge with a highly pathogenic Mtb strain (Erdman strain). Although Kaushal *et al.*¹² have reported very good protection in RMs against a less pathogenic Mtb strain (CDC1551) with high-dose, aerosol ‘vaccination’ of a live, attenuated mycobacterium-based TB vaccine strain (MtbΔSigH), Mtb challenge in these studies occurred only 8 weeks after aerosol vaccine administration, a time at which the replicating MtbΔSigH strain would still be present in lungs of vaccinated RMs and both innate and adaptive immunity would presumably be at or near peak levels. In contrast, the potent RhCMV/TB-vaccine-mediated protection demonstrated here against low-dose challenge with the highly pathogenic Erdman strain of Mtb occurred as long as 55 weeks following initial vaccination, and 40 weeks following boosting of the subcutaneously administered vaccine, consistent with establishment of long-term protection.

The working hypothesis upon which CMV vaccine vector development is based on relates to the ability of these persistent vectors to elicit and maintain effector-differentiated (‘effector memory’), insert-specific CD4⁺ and CD8⁺ T cell responses in mucosal effector sites and in secondary lymphoid tissues, as well as circulating in the blood, that are pre-positioned to intercept mucosally acquired pathogens at the very onset of infection. Although it is difficult to definitively establish the mechanism of action in a vaccine protection study, the available data are consistent with the operation of this effector memory hypothesis in the RhCMV/TB-vaccine-mediated control of Mtb infection. Consistent with previous work on RhCMV/SIV vaccines^{22–24}, RhCMV/TB vectors elicited robust circulating and tissue-based CD4⁺ and CD8⁺ T cell responses (but essentially no insert-specific Ab responses), with both the CD4⁺ and CD8⁺ T cell responses in blood being highly effector memory biased (T_{TREM} + T_{EM} for CD4⁺; T_{EM} for CD8⁺). Although there are other semi-innate and innate cell types in the lung and lung-draining LNs that could potentially participate in protection against Mtb³⁸, the effector-differentiated, Mtb-specific CD4⁺ and CD8⁺ T cells are essentially the only adaptive immune responses detected in RhCMV/TB-vaccinated RMs. Moreover, protection appeared very early in many RMs—before the onset of detectable pathology and early enough to reduce, and even abrogate, the potent interferon-driven innate immune response to Mtb infection. This protection also occurred in the absence of a true anamnestic response, consistent with the concept of protection being mediated by established effectors already ‘in place’ or rapidly recruited at the time of challenge. It is also noteworthy that the most pronounced adaptive immune difference between RhCMV/TB-elicited and the (nonprotective) BCG-elicited T cell responses was in the Mtb-specific CD4⁺ T cell responses before challenge, in particular in their differentiation and functional potential, with the i.d. administered BCG vaccine eliciting predominantly monofunctional, central memory responses versus polyfunctional (TNF- and IFN-γ-producing) effector-differentiated (T_{EM} + T_{TREM}) responses by the RhCMV/TB vaccine. With respect to Mtb-specific CD8⁺ T cell responses, the protection afforded by vaccination with the 68-1.2 RhCMV/TB vector indicates that the unconventional MHC-II and MHC-E-restricted CD8⁺ T cells are not required for protection, and suggests that either conventional or

unconventional CD8⁺ T cell responses can contribute to protection, or that protection is independent of CD8⁺ T cells altogether.

The observation that outcome heterogeneity among RhCMV/TB-vaccinated RMs was not predicted by the pre-challenge magnitude of RhCMV/TB-elicited, TNF- and/or IFN-γ-defined, CD4⁺ or CD8⁺ T cell responses in blood, BAL fluid or LNs does not refute the effector memory hypothesis, as these sampling sites and the ICS assay read-out may not accurately reflect the frequency and function of resident memory responses in lung and lung-draining LN that are likely the relevant population for earliest immune control of infection and thus for protection³⁹. In contrast to T cell responses that either continuously recirculate (central memory responses) or have a required blood-borne component (classic anamnestic memory responses), effector memory responses are regulated locally, are not well represented by blood measurements, are difficult to characterize *ex vivo*, and are not uniform across tissue compartments^{40,41}. It should also be noted that a correlation between the magnitude of the pre-challenge Mtb-insert-specific T cell response and subsequent protection would be expected only if this T cell response magnitude was the major limiting component of the protective immune response. Because CD4⁺ and CD8⁺ T cells are not thought to directly kill Mtb, but rather to work through innate immune (primarily phagocytic) effectors, it is possible that a required innate immune co-effector component is the limiting factor that primarily determines whether an individual RhCMV/TB vaccine recipient will be completely protected, partially protected or not at all protected after challenge. In this regard, the gene expression levels that were identified in the pre-challenge transcriptomic analysis of whole blood to be predictive of the RhCMV/TB vaccine effect preferentially included genes expressed by neutrophils and were associated with innate immunity and neutrophil degranulation gene pathways, including genes that encoded neutrophil granule effector molecules (*MMP8* and *CTSG*) (Fig. 6). This protection signature was somewhat unexpected, as in overt TB disease, neutrophils have been primarily associated with TB pathogenesis, mediating tissue destruction, necrosis and cavitation, and providing a pro-Mtb milieu, but not with effective Mtb killing^{42–45}. However, some studies have demonstrated an ability of neutrophils to kill, restrict the growth of, or trap Mtb (preventing its spread), raising the question of whether the role of the neutrophil in TB immunity and pathogenesis is both timing and context dependent^{7,46–49}. Indeed, one study demonstrated an inverse correlation between neutrophil counts and the risk of TB infection in contacts of patients who were diagnosed with pulmonary TB⁴⁷, consistent with an early protective role for this cell population.

Our demonstration that neutrophil gene expression patterns, but not neutrophil counts themselves, predicted outcome in RhCMV/TB-vaccinated RMs but not in unvaccinated and BCG-vaccinated RMs suggested that neutrophils might be important co-effectors for RhCMV/TB-vaccine-elicited T cell responses and that their differentiation or activation state determined, at least in part, their ability to contribute to RhCMV/TB-vaccine-mediated protection. Notably, it appears that the protection-associated transcriptomic signature in neutrophils primarily delineates RhCMV/TB-vaccinated RMs destined for complete or nearly complete protection from those with partial or no protection (Fig. 6), suggesting that the contribution of ‘primed’ neutrophils to protection occurs very early after challenge and wanes thereafter. The extent to which this protective neutrophil differentiation or activation state is related to RhCMV/TB vaccination, monkey genetics or immune events at the time of challenge remains to be determined; however, it is notable that BCG

vaccination 6 weeks prior to administration of the RhCMV/TB vaccine appeared to deleteriously modify the expression of several of the protection-associated genes (Fig. 6), suggesting that innate immune modulation might account for the apparent antiprotective effect of administering BCG before RhCMV/TB vaccination. Additional studies to determine the effect of remote (neonatal) BCG vaccination on RhCMV/TB-vector-mediated protection in adolescent and adult RMs will be required to clarify the potential clinical significance of this putative antagonistic effect in at-risk human populations who have previously received the BCG vaccine at birth.

In summary, the data presented here demonstrate that RhCMV-based vaccines manifest significant protection against aggressive Erdman-strain-mediated TB in highly susceptible RMs. Although delineation of the specific immunological mechanisms responsible for protection in RhCMV/TB-vaccinated individuals will require additional study, the nature of RhCMV/TB vector immunogenicity and the dynamics of protection after challenge suggest that protection is based on both the ability of this persistent viral vector to elicit and maintain Mtb-specific effector-differentiated circulating and resident memory T cell responses and on a conducive innate immune state at the time of Mtb challenge that might also be vaccine related^{50,51}. Notably, it has been documented in natural CMV infection that the robust T_{TrEM} and T_{EM} cell responses elicited by this virus are maintained for life^{19,20}. To our knowledge, CMV is unique in this ability, and recent data indicate that strategically attenuated CMV vectors, which are potentially safe enough for clinical translation, maintain this unique immunogenicity (S.G.H., K.F. and L.J.P., unpublished data). How the above-mentioned putative interaction between CMV-vaccine-elicited T_{TrEM} and T_{EM} cell responses and BCG- or Mtb-elicited immune regulation will play out over clinically relevant timeframes in people remains to be determined. However, the ability of RhCMV/TB vaccination to completely prevent development of TB disease in more than 40% of vaccinated RMs and to provide a nearly 70% overall vaccine effect offers promise that a human CMV/TB vaccine might be effective in preventing pulmonary TB in adolescents and adults⁵², which could thereby contribute to ending the global TB epidemic.

METHODS

Methods, including statements of data availability and any associated accession codes and references, are available in the [online version of the paper](#).

Note: Any Supplementary Information and Source Data files are available in the [online version of the paper](#).

ACKNOWLEDGMENTS

We thank C. Kahl, S. Hagen, J. Bae, I. Pelletier, Y. Guo, E.M. Borst, L.S. Uebelhoer and J. Womack for technical assistance, C. Scanga and J. Flynn for guidance on the RM model of TB (including sharing of NHP protocols and provision of Mtb challenge stocks), P. Barry (University of California, Davis) and T. Shenk (Princeton University) for the 68-1 and 68-1.2 BACs, respectively, J. Flynn (University of Pittsburgh) for Mtb Erdman, W. Hanekom, L. Stuart and D. Barber for helpful discussions, D. Casimiro for manuscript review, J. Strussenberg for management of the BSL3 facility, L. Boshears for administrative assistance and A. Townsend for figure preparation. This work was supported by AERAS, the Bill and Melinda Gates Foundation (grant no. OPP1087783; A.A. and D.E.Z.) and the US National Institutes of Health (NIH; grant no. U19 AI106761 (A.A.), P51 OD011092 (ONPRC); U42 OD010426 (ONPRC)).

AUTHOR CONTRIBUTIONS

S.G.H. planned animal experiments and supervised all immunological and virological studies and data analysis; G.X. and J.C.F. processed monkey samples and tissues and performed immunological and bacteriological analyses, assisted by R.M.G., C.M.H., A.B.V., E.A., K.T.R., A.N.S., P.R., L.H., H.P. and M.S.L.;

A.W.S. performed assay development and supervised flow cytometry; K.F., D.M., E.E.M., M.M. and M.A.J. designed, constructed and/or validated the RhCMV/TB vectors used in the study; A.W.L. supervised all animal procedures, including CT scanning, assisted by S.L.P., J.M.T., M.F., C.A., and R.C.Z.; M.K.A. planned and provided overall supervision of monkey protocols, interpreted CT scans, performed all necropsies and interpreted both gross pathology and histopathology; D.J.L. designed experimental approaches and reviewed data; M.S., A.B. and T.G.E. contributed to data interpretation and/or study design; L.L. performed the antibody assays under the supervision of G.A.; J.V., J.M.B. and S.S. processed samples and data for transcriptomic analysis; D.E.Z. planned, executed and interpreted the transcriptomics analysis, assisted by L.M.A., S.S., and A.A.; P.T.E. planned and performed all statistical analyses; L.J.P. conceived the RhCMV vector strategy, planned and supervised all experiments and data analysis, and wrote the manuscript, assisted by S.G.H., P.T.E., D.E.Z. and M.K.A.

COMPETING FINANCIAL INTERESTS

The authors declare competing financial interests: details are available in the [online version of the paper](#).

Reprints and permissions information is available online at <http://www.nature.com/reprints/index.html>. Publisher's note: Springer Nature remains neutral with regard to jurisdictional claims in published maps and institutional affiliations.

- Cambier, C.J., Falkow, S. & Ramakrishnan, L. Host evasion and exploitation schemes of *Mycobacterium tuberculosis*. *Cell* **159**, 1497–1509 (2014).
- Orme, I.M., Robinson, R.T. & Cooper, A.M. The balance between protective and pathogenic immune responses in the TB-infected lung. *Nat. Immunol.* **16**, 57–63 (2015).
- Shaler, C.R., Horvath, C.N., Jeyanathan, M. & Xing, Z. Within the enemy's camp: contribution of the granuloma to the dissemination, persistence and transmission of *Mycobacterium tuberculosis*. *Front. Immunol.* **4**, 30 (2013).
- Pai, M. *et al.* Tuberculosis. *Nat. Rev. Dis. Primers* **2**, 16076 (2016).
- Comas, I. *et al.* Human T cell epitopes of *Mycobacterium tuberculosis* are evolutionarily hyperconserved. *Nat. Genet.* **42**, 498–503 (2010).
- Comas, I. *et al.* Out-of-Africa migration and Neolithic coexpansion of *Mycobacterium tuberculosis* with modern humans. *Nat. Genet.* **45**, 1176–1182 (2013).
- Dorhoi, A. & Kaufmann, S.H. Pathology and immune reactivity: understanding multidimensionality in pulmonary tuberculosis. *Semin. Immunopathol.* **38**, 153–166 (2016).
- Hawn, T.R. *et al.* Tuberculosis vaccines and prevention of infection. *Microbiol. Mol. Biol. Rev.* **78**, 650–671 (2014).
- Kaufmann, S.H. Future vaccination strategies against tuberculosis: thinking outside the box. *Immunity* **33**, 567–577 (2010).
- Griffiths, K.L. *et al.* Targeting dendritic cells to accelerate T cell activation overcomes a bottleneck in tuberculosis vaccine efficacy. *Nat. Commun.* **7**, 13894 (2016).
- Barclay, W.R. *et al.* Protection of monkeys against airborne tuberculosis by aerosol vaccination with bacillus Calmette–Guerin. *Am. Rev. Respir. Dis.* **107**, 351–358 (1973).
- Kaushal, D. *et al.* Mucosal vaccination with attenuated *Mycobacterium tuberculosis* induces strong central memory responses and protects against tuberculosis. *Nat. Commun.* **6**, 8533 (2015).
- Verreck, F.A.W. *et al.* Variable BCG efficacy in rhesus populations: pulmonary BCG provides protection where standard intradermal vaccination fails. *Tuberculosis (Edinb.)* **104**, 46–57 (2017).
- Jeyanathan, M. *et al.* AdHu5Ag85A respiratory mucosal boost immunization enhances protection against pulmonary tuberculosis in BCG-primed nonhuman primates. *PLoS One* **10**, e0135009 (2015).
- Darrah, P.A. *et al.* Aerosol vaccination with AERAS-402 elicits robust cellular immune responses in the lungs of rhesus macaques but fails to protect against high-dose *Mycobacterium tuberculosis* challenge. *J. Immunol.* **193**, 1799–1811 (2014).
- Verreck, F.A. *et al.* MVA.85A boosting of BCG and an attenuated, *phoP*-deficient *M. tuberculosis* vaccine both show protective efficacy against tuberculosis in rhesus macaques. *PLoS One* **4**, e5264 (2009).
- Tameris, M.D. *et al.* Safety and efficacy of MVA85A, a new tuberculosis vaccine, in infants previously vaccinated with BCG: a randomized, placebo-controlled phase 2b trial. *Lancet* **381**, 1021–1028 (2013).
- Tameris, M. *et al.* The candidate TB vaccine, MVA85A, induces highly durable T_H1 responses. *PLoS One* **9**, e87340 (2014).
- Jarvis, M.A., Hansen, S.G., Nelson, J.A., Picker, L.J. & Fröh, K. in *Cytomegaloviruses: From Molecular Pathogenesis to Intervention* Vol. 2 (ed. Reddehase, M.J.) 450–462 (Caister Academic Press, 2013).
- Cicin-Sain, L. *et al.* Cytomegalovirus-specific T cell immunity is maintained in immunosenescent rhesus macaques. *J. Immunol.* **187**, 1722–1732 (2011).
- Sylwester, A.W. *et al.* Broadly targeted human-cytomegalovirus-specific CD4⁺ and CD8⁺ T cells dominate the memory compartments of exposed subjects. *J. Exp. Med.* **202**, 673–685 (2005).
- Hansen, S.G. *et al.* Effector memory T cell responses are associated with protection of rhesus monkeys from mucosal simian immunodeficiency virus challenge. *Nat. Med.* **15**, 293–299 (2009).
- Hansen, S.G. *et al.* Profound early control of highly pathogenic SIV by an effector memory T cell vaccine. *Nature* **473**, 523–527 (2011).

24. Hansen, S.G. *et al.* Immune clearance of highly pathogenic SIV infection. *Nature* **502**, 100–104 (2013).
25. Hansen, S.G. *et al.* Broadly targeted CD8⁺ T cell responses restricted by major histocompatibility complex E. *Science* **351**, 714–720 (2016).
26. Scanga, C.A. & Flynn, J.L. Modeling tuberculosis in nonhuman primates. *Cold Spring Harb. Perspect. Med.* **4**, a018564 (2014).
27. Sharpe, S. *et al.* Ultra-low-dose aerosol challenge with *Mycobacterium tuberculosis* leads to divergent outcomes in rhesus and cynomolgus macaques. *Tuberculosis* **96**, 1–12 (2016).
28. Gormus, B.J., Blanchard, J.L., Alvarez, X.H. & Didier, P.J. Evidence for a rhesus monkey model of asymptomatic tuberculosis. *J. Med. Primatol.* **33**, 134–145 (2004).
29. Sibley, L. *et al.* Route of delivery to the airway influences the distribution of pulmonary disease but not the outcome of *Mycobacterium tuberculosis* infection in rhesus macaques. *Tuberculosis* **96**, 141–149 (2016).
30. Mothé, B.R. *et al.* The TB-specific CD4⁺ T cell immune repertoire in both cynomolgus and rhesus macaques largely overlap with humans. *Tuberculosis (Edinb.)* **95**, 722–735 (2015).
31. Langermans, J.A. *et al.* Divergent effect of bacillus Calmette–Guérin (BCG) vaccination on *Mycobacterium tuberculosis* infection in highly related macaque species: implications for primate models in tuberculosis vaccine research. *Proc. Natl. Acad. Sci. USA* **98**, 11497–11502 (2001).
32. Hsu, T. *et al.* The primary mechanism of attenuation of bacillus Calmette–Guerin is a loss of secreted lytic function required for invasion of lung interstitial tissue. *Proc. Natl. Acad. Sci. USA* **100**, 12420–12425 (2003).
33. Hansen, S.G. *et al.* Cytomegalovirus vectors violate CD8⁺ T cell epitope recognition paradigms. *Science* **340**, 1237874 (2013).
34. Zak, D.E. *et al.* A blood RNA signature for tuberculosis disease risk: a prospective cohort study. *Lancet* **387**, 2312–2322 (2016).
35. Cliff, J.M., Kaufmann, S.H., McShane, H., van Helden, P. & O'Garra, A. The human immune response to tuberculosis and its treatment: a view from the blood. *Immunol. Rev.* **264**, 88–102 (2015).
36. Berry, M.P. *et al.* An interferon-inducible neutrophil-driven blood transcriptional signature in human tuberculosis. *Nature* **466**, 973–977 (2010).
37. Kaforou, M. *et al.* Detection of tuberculosis in HIV-infected and uninfected African adults using whole-blood RNA expression signatures: a case–control study. *PLoS Med.* **10**, e1001538 (2013).
38. De Libero, G., Singhal, A., Lepore, M. & Mori, L. Nonclassical T cells and their antigens in tuberculosis. *Cold Spring Harb. Perspect. Med.* **4**, a018473 (2014).
39. Rayner, E.L. *et al.* Early lesions following aerosol infection of rhesus macaques (*Macacamulatta*) with *Mycobacterium tuberculosis* strain H37RV. *J. Comp. Pathol.* **149**, 475–485 (2013).
40. Steinert, E.M. *et al.* Quantifying memory CD8 T cells reveals regionalization of immunosurveillance. *Cell* **161**, 737–749 (2015).
41. Thome, J.J. & Farber, D.L. Emerging concepts in tissue-resident T cells: lessons from humans. *Trends Immunol.* **36**, 428–435 (2015).
42. Dallenga, T. & Schaible, U.E. Neutrophils in tuberculosis—first line of defense or booster of disease and targets for host-directed therapy? *Pathog. Dis.* **74**, ftw012 (2016).
43. Mishra, B.B. *et al.* Nitric oxide prevents a pathogen-permissive granulocytic inflammation during tuberculosis. *Nat. Microbiol.* **2**, 17072 (2017).
44. Ong, C.W. *et al.* Neutrophil-derived MMP-8 drives AMPK-dependent matrix destruction in human pulmonary tuberculosis. *PLoS Pathog.* **11**, e1004917 (2015).
45. Mattila, J.T., Maiello, P., Sun, T., Via, L.E. & Flynn, J.L. Granzyme B-expressing neutrophils correlate with bacterial load in granulomas from *Mycobacterium tuberculosis*-infected cynomolgus macaques. *Cell. Microbiol.* **17**, 1085–1097 (2015).
46. Lyadova, I.V. Neutrophils in tuberculosis: heterogeneity shapes the way? *Mediators Inflamm.* **2017**, 8619307 (2017).
47. Martineau, A.R. *et al.* Neutrophil-mediated innate immune resistance to mycobacteria. *J. Clin. Invest.* **117**, 1988–1994 (2007).
48. Warren, E., Teskey, G. & Venketaraman, V. Effector mechanisms of neutrophils within the innate immune system in response to *Mycobacterium tuberculosis* infection. *J. Clin. Med.* **6**, E16 (2017).
49. Seiler, P. *et al.* Early granuloma formation after aerosol *Mycobacterium tuberculosis* infection is regulated by neutrophils via CXCR3-signaling chemokines. *Eur. J. Immunol.* **33**, 2676–2686 (2003).
50. Jeyanathan, M. *et al.* Differentially imprinted innate immunity by mucosal boost vaccination determines antituberculosis immune protective outcomes, independent of T cell immunity. *Mucosal Immunol.* **6**, 612–625 (2013).
51. Beverley, P.C. *et al.* A novel murine cytomegalovirus vaccine vector protects against *Mycobacterium tuberculosis*. *J. Immunol.* **193**, 2306–2316 (2014).
52. Knight, G.M. *et al.* Impact and cost-effectiveness of new tuberculosis vaccines in low- and middle-income countries. *Proc. Natl. Acad. Sci. USA* **111**, 15520–15525 (2014).
53. Obermoser, G. *et al.* Systems-scale interactive exploration reveals quantitative and qualitative differences in response to influenza and pneumococcal vaccines. *Immunity* **38**, 831–844 (2013).
54. Fabregat, A. *et al.* The Reactome pathway Knowledgebase. *Nucleic Acids Res.* **44** (D1), D481–D487 (2016).
55. Clemmensen, S.N. *et al.* Olfactomedin 4 defines a subset of human neutrophils. *J. Leukoc. Biol.* **91**, 495–500 (2012).
56. Ambrose, L.R., Morel, A.S. & Warrens, A.N. Neutrophils express CD52 and exhibit complement-mediated lysis in the presence of alemtuzumab. *Blood* **114**, 3052–3055 (2009).

ONLINE METHODS

Rhesus macaques. Sixty-five purpose-bred, pedigreed, male RMs (*Macaca mulatta*) of Indian genetic background were used in our studies. At assignment, these RMs were specific-pathogen free (SPF) as defined by being free of macacine herpesvirus 1, D-type simian retrovirus, simian T lymphotropic virus type 1, simian immunodeficiency virus and Mtb; however, all were naturally RhCMV-infected. All of the RMs used in this study were housed at the Oregon National Primate Research Center (ONPRC) in animal biosafety level (ABSL)-2 (vaccine phase) and ABSL-3 rooms (challenge phase) with autonomously controlled temperature, humidity and lighting. The RMs were single-cage-housed due to the infectious nature of the study and had visual, auditory and olfactory contact with other animals. Because the RMs were single-cage-housed, an enhanced enrichment plan was designed and overseen by NHP behavior specialists. The RMs were fed commercially prepared primate chow (Purina Lab Diet: Fiber-Balanced Monkey Jumbo, 5000; High Protein Monkey Diet, 5045) twice daily and received supplemental fresh fruit or vegetables daily. Fresh, potable water was provided via automatic water systems. All of the RMs were observed twice daily to assess appetite, attitude, activity level, hydration status and evidence of disease (tachypnea, dyspnea and coughing). Physical exams, including body weight and complete blood counts, were performed at all protocol time points. RM care and all of the experimental protocols and procedures were approved by the ONPRC Institutional Animal Care and Use Committee (IACUC). The ONPRC is accredited as a Category 1 facility by the American Association for Accreditation of Laboratory Animal Care (AAALAC) and has an approved Assurance (#A3304-01) for the care and use of animals on file with the Office for Protection from Research Risks at NIH. The IACUC adheres to national guidelines established in the Animal Welfare Act (7 U.S.C. Sections 2131–2159) and the Guide for the Care and Use of Laboratory Animals⁵⁷ as mandated by the US Public Health Service Policy.

Animal procedures. The RMs were sedated with ketamine-HCl or Telazol for intradermal and subcutaneous vaccine administration, venipuncture, BAL, LN biopsy, intrabronchial Mtb inoculation and CT procedures. Mtb Erdman (kindly provided by J. Flynn, University of Pittsburgh) was diluted in saline and lightly sonicated, and the bacteria were delivered to a segmental bronchus in the right caudal lung lobe using a bronchoscope. The RMs in Study 1 and Study 2 received 25 and 10 CFUs, respectively, in a volume of 1 ml (ref. 58). Pre- and post-challenge axial CT scans (2.5-mm slices) were obtained using a multisection CT scanner using helical technique, collimation of 3 mm and pitch of 1.5 (CereTom, Neurologica Corp., Danvers, MA) and were reconstructed as 1.25-mm slices to improve detection sensitivity^{59,60}. Nonionic iodinated contrast (Isovue 370, 1–2 ml/kg, Bracco Diagnostics, Princeton, NJ) was administered intravenously at a rate of 1–2 ml/s. CT scans were obtained with 120 kVp and 200 mA. All RMs were imaged pre-challenge, at 2-week intervals for the duration of the studies and immediately before necropsy. Scans were interpreted by a veterinarian who was blinded to the study group of the subject. Lesion area in sequential scans was determined from transverse slices through entire lung fields using the IMPAX 6.5.5.3020 software area tool (AGFA HealthCare N.V., Mortsel, Belgium), and lesion volume was determined by multiplying the area by 1.25. One RM developed extensive bilateral miliary disease with an estimated lesion volume >200,000 mm³, and no further attempts to estimate lesion volume were made in this animal.

Necropsy. The humane criteria for removing RMs with end-stage TB from the studies were as follows: (i) marked lethargy, (ii) severe dyspnea at rest and/or failure to maintain adequate oxygenation (85%) based on pulse oximetry or blood gas analysis, (iii) hemoptysis, (iv) weight loss (>15% in 2 weeks; >25% over any time course in an adult animal), (v) hypothermia <96°F with supplemental heating, (vi) persistent anemia (<20% for 2 weeks), (vii) dehydration that was unresponsive to oral rehydration therapy for 3 d, (viii) nonresponsiveness to therapy for spontaneous disease conditions, (ix) poor appetite, requiring more than three orogastric tube feedings in 7 d, (x) obtundation, (xi) neurologic deficits and (xii) persistent self-injurious behavior that was unresponsive to a change in location or enrichment. RMs that manifested one or more of these end-stage criteria were immediately euthanized and taken to

necropsy. RMs that remained clinically well after week 16 p.i. were randomized and scheduled for euthanasia and necropsy at the rate of two per week. There were three exceptions to this general rule of necropsy initiated by end-stage disease criteria or randomization (three necropsies that are designated as “other” in Fig. 1a). One non-end-stage RM (D1) in Study 1 was euthanized on the same day as an end-stage RM because the IACUC does not permit housing a single RM alone in a room. Two additional RMs (N1 and N3) in Study 1 were euthanized because of failure to maintain adequate oxygenation following a BAL procedure that was not attributable to end-stage Mtb disease. To avoid this issue in Study 2, BAL was not performed after challenge.

At the humane or scheduled end point, the RMs were euthanized with a sodium pentobarbital overdose (>50 mg/kg) and exsanguinated via the distal aorta. The necropsy procedure included complete gross pathological evaluation of abdominal organs and tissues and of the brain before entering the thoracic cavity, to avoid contamination. Macroscopic granulomas in the liver, spleen, kidney and brain were counted, measured and photographed in serial 5-mm tissue slices, whereas granulomas occurring in extrathoracic LNs, the gastrointestinal tract and the soft tissues were collected, measured and photographed with minimum sectioning and given a numeric point value score using a semiquantitative grading system (Supplementary Fig. 3). Granulomas (≤10) occurring in these tissues were bisected, one half was collected in tubes with sterile medium for Mtb culture (see below), and the remaining half was immersed in 10% neutral-buffered formalin for histological analysis. Representative granulomas were selected for Mtb culture and histology from tissues with >10 granulomas. Single, small granulomas (≤1 mm) were used entirely for bacteriology. If no granulomas were identified, then representative samples of selected tissues (see below) were submitted for Mtb culture. Representative samples of all abdominal and mediastinal organs and associated major LN groups, and both the brain and spinal cord, were collected and then fixed in 10% neutral-buffered formalin for histological analysis. Additional samples from these tissues were collected for mononuclear cell isolation. The pleura and thoracic wall were examined after entering the thoracic cavity, and macroscopic granulomas and adhesions were collected, counted, measured, photographed, scored as described (Supplementary Fig. 3), and sampled for bacteriology and histology. The thoracic viscera were removed *en bloc* and then transferred to a sterile cutting board for examination and dissection. Extreme care was taken to avoid Mtb contamination of thoracic tissues by spillage of granuloma contents during dissection, and this was accomplished in all but one RM in which gross spillage of granuloma contents was observed upon opening the thoracic cavity. The heart was removed and examined, and pulmonary and mediastinal LNs and individual lung lobes were dissected free, weighed and photographed. LNs were divided into samples for Mtb culture, histopathology and mononuclear cell isolation (with Mtb culture prioritized if the amount of tissue was limiting). Macroscopic granulomas in individual lung lobes were counted, measured, photographed and scored in serial 5-mm tissue slices. Samples for Mtb culture from the right- and left-lung slices were harvested using a nonbiased, stereological sampling method⁶¹. Briefly, an opaque plastic 96-hole strip-tube rack was placed over the adjacent lung slices, and individual 5-mm lung tissue cores (30 from the right lung and ten from the left lung) were collected through these the openings in the rack (irrespective of any gross pathology) in a consistent pattern across all of the monkeys in the study. These stereologically obtained (essentially random) lung cores were bisected, and one-half was processed for bacteriology, whereas the remaining half was immersed in 10% neutral-buffered formalin for histological analysis. In addition, as indicated above, extensive representative samples of all lung lobes and lung-draining LNs, all abdominal and mediastinal organs and tissues, and all major non-lung-draining LN groups were collected and immersed in 10% neutral-buffered formalin for histological analysis. Tissues for histological analysis were routinely processed and embedded in paraffin. Sections (6 mm) were stained with hematoxylin and eosin. In total, between 100 and 120 tissue blocks were examined by a veterinary pathologist for each monkey necropsy, ~50 of which focused on the lung, trachea or major bronchi, and lung-draining LNs, and the remainder were for the other non-pulmonary tissues. Selected tissues were stained by the Ziehl–Neelsen method for acid-fast bacteria.

Vaccines. The 68-1 and 68-1.2 RhCMV/TB vectors were constructed by bacterial artificial chromosome (BAC) recombinering and were reconstituted and amplified into vector preparations as previously described^{22–24,33}. The Mtb Ags to be included in these vectors were selected by a bioinformatics selection criteria starting with the scoring of 4,000 Mtb open-reading frames (ORFs) by 11 criteria⁶². Those criteria included immunogenicity, vaccine efficacy, expression in granulomas, ability for secretion and role in hypoxic survival. The top candidates were then further screened by a deeper bioinformatics analysis of predicted T cell epitopes and curated to include antigens that are active during different stages of TB infection. In addition, all of the antigens had been shown to be at least partially protective in a mouse challenge model. The final choice of nine Mtb proteins for the vaccine inserts included three representative proteins from so-called acute-phase (85A, 85B and ESAT-6), latency (Rv1733, Rv3407 and Rv2626) and resuscitation (Rpf A, Rpf C and Rpf D) classes of Mtb Ags. These nine Ags were expressed in four different RhCMV/TB vectors (to be used in combination) for both the 68-1 and 68-1.2 backbones, as follows: (i) Ag85A/Ag85B/Rv3407 (GenBank [KY611401](#)), (ii) Rv1733/Rv2626 (GenBank [KY611402](#)), (iii) Rpf A/Rpf C/Rpf D (GenBank [KY611403](#)), and (iv) Ag85B/ESAT-6 (GenBank [KY611404](#)). The GenBank accession number corresponds to the sequences as they are found in the final vectors. Polyprotein numbers 1–3 were inserted into the nonessential Rh211 ORF under the control of the murine CMV immediate early (IE) promoter. Polyprotein 4 was inserted in the same region of the RhCMV genome but under the control of the promoter from the eukaryotic translation elongation factor 1 alpha 1 (*EEF1A1*) gene (Supplementary Fig. 1a). For the single six-Ag-expressing, 68-1 RhCMV/TB vector, a single polyprotein insert consisting of two Ags from each of three classes described above (acute-phase: ESAT-6 and Ag85A; latency: Rv3407 and Rv2626; resuscitation: RpfA and RpfD; GenBank [KY611405](#)) was used to replace the non-essential Rh107 gene, placing its expression under the control of the endogenous Rh107 promoter (Supplementary Fig. 1a). All BACs were analyzed by restriction digestion to confirm genomic integrity and were further examined by next-generation sequencing (NGS) on an Illumina MiSeq sequencer to ensure the absence of any unintended mutations in the transgene. Full genome sequences of viral DNA isolated from vaccine stocks used in the presented study (68-1 RhCMV/85A/85B/Rv3407 (MF468139); 68-1.2 RhCMV/85A/85B/Rv3407 (MF468141); 68-1.2 RhCMV/85B/ESAT-6 (MF468142); 68-1.2 RhCMV/Rpf A/Rpf C/Rpf D (MF468143); 68-1.2 RhCMV/Rv1733c/Rv2626c (MF468144); 68-1 RhCMV/Rpf A/Rpf C/Rpf D (MF468145) and 68-1 RhCMV/Rv1733c/Rv2626c (MF468146)) or full genome sequences of the BAC of the mutant used to derive the vaccine stocks (68-1 RhCMV/85B/ESAT-6 (MF468140) and 68-1 ΔRh107 RhCMV/TB-6Ag (MF468147)) were submitted to GenBank. To reconstitute the vaccine vectors, the BACs were electroporated into telomerized or primary rhesus fibroblasts and kept in culture until full cytopathic effect was achieved. At this point, transgene expression was confirmed by immunoblot analysis of lysates from infected cells, and vaccine stocks were generated by the ONPRC Molecular Virology Support Core. Overall genomic integrity and transgene expression of the final vaccine stocks were confirmed by immunoblots, NGS and pilot immunogenicity studies in RMs. Expression of the ORFs neighboring the TB Ag insertion site was confirmed by RT-PCR. RhCMV/TB vector stocks were titered using primary rhesus fibroblasts in an end-point dilution assay. Study 1 and Study 2 RMs were vaccinated by subcutaneous administration of 5×10^6 plaque-forming units (pfu) of each of the designated RhCMV/TB vectors. For the RMs receiving the four-vector set, each vector was administered in a separate limb (right arm, left arm, right leg and left leg). The RMs were given the test vaccines twice, with the second dose (homologous boost) administered 15 weeks (Study 1) or 14 weeks (Study 2) after the first dose. The BCG vaccine (Danish strain 1331; batch no. 111005A) was obtained from the Statens Serum Institute (Copenhagen, Denmark) and was reconstituted per the manufacturer's instructions (diluent batch no. 386587B). The RMs were BCG-vaccinated by intradermal administration of 100 μl of vaccine containing 5.5×10^5 CFUs into the mid-back.

Immunological assays. Mtb-specific CD4⁺ and CD8⁺ T cell responses were measured in blood, BAL fluid and tissues by flow cytometric ICS, as previously described in detail^{22,25,33}. Briefly, mononuclear-cell preparations from blood, BAL fluid or tissue were incubated at 37 °C in a humidified 5% CO₂ atmosphere with overlapping, consecutive 15-mer peptide mixes (overlap of 11 amino

acids) comprising these proteins, or individual 15-mer peptides from these proteins, and monoclonal antibodies to the co-stimulatory molecules CD28 and CD49d (eBioscience) for 1 h, followed by addition of brefeldin A (Sigma-Aldrich) for an additional 8 h. Co-stimulation without antigenic peptides served as a background control. As previously described²⁵, the MHC restriction (MHC-Ia, MHC-E, MHC-II) of a peptide-specific response was determined by pre-incubating isolated mononuclear cells for 1 h at room temperature (before adding peptides and incubating per the standard ICS assay) with the following blockers: (i) the pan anti-MHC-I monoclonal Ab (mAb) W6/32 (10 mg/ml), (ii) the MHC-II-blocking CLIP peptide (MHC-II-associated invariant chain, amino acids 89–100; 20 μM), and (iii) the MHC-E-blocking VL9 peptide (VMAPRTLTL; 20 μM). Blocking reagents were not washed, but remained throughout the assay. Following incubation, stimulated cells were fixed, permeabilized and stained as previously described^{22,25,33} using combinations of the following fluorochrome-conjugated mAbs (for antibody information, see **Supplementary Methods**): SP34-2 (CD3; Pacific Blue, Alexa700), L200 (CD4; AmCyan, BV510), SK-1 (CD8α; PerCP-Cy5.5), MAB11 (TNF; FITC, PE), B27 (IFN-γ; APC), FN50 (CD69; PE, PE-TexasRed), B56 (Ki-67; FITC), and in polycytokine analyses, JES6-5H4 (IL-2; PE, PE Cy-7). To determine the cell surface phenotype of Mtb-specific CD4⁺ and CD8⁺ T cells, mononuclear cells were stimulated as described above, except that the CD28 co-stimulatory mAb was used as a fluorochrome conjugate to allow CD28 expression levels to be later assessed by flow cytometry; in these experiments, cells were surface-stained after incubation for lineage markers CD3, CD4, CD8, CD95 and CCR7 (see below for mAb clones) before fixation and permeabilization, and were then subjected to intracellular staining for response markers (CD69, IFN-γ, TNF; note that brefeldin A treatment preserves the pre-stimulation cell-surface expression phenotype of phenotypic markers examined in this study). Data were collected on an LSR-II (BD Biosciences). Analysis was performed using FlowJo software (Tree Star). In all analyses, gating on the lymphocyte population was followed by the separation of the CD3⁺ T cell subset and progressive gating on the CD4⁺ and CD8⁺ T cell subsets. Antigen-responding cells in both CD4⁺ and CD8⁺ T cell populations were determined by their intracellular expression of CD69 and one or more cytokines (either or both of IFN-γ and TNF; ± IL-2 in polycytokine analyses). After subtracting the background values, the raw response frequencies above the assay limit of detection were 'memory-corrected' (adjusted to reflect the percentage of cells responding out of the memory population), as previously described^{22,23} using combinations of the following fluorochrome-conjugated mAbs to define the memory versus naive subsets SP34-2 (CD3; Alexa700, PerCP-Cy5.5), L200 (CD4; AmCyan), SK-1 (CD8-α; APC, PerCP-Cy-5.5), MAB11 (TNF; FITC), B27 (IFN-γ; APC), FN50 (CD69; PE), CD28.2 (CD28; PE-TexasRed), DX2 (CD95; PE), 15053 (CCR7; Pacific Blue) and B56 (Ki-67; FITC) (for antibody information, see **Supplementary Methods**). As previously described²¹, the background of the assay was determined by measurement of the net response to the Ags of interest in a cohort of monkeys that had never been exposed to these Ags. We, conservatively, used 4 s.d. above the mean of these background values as our cut-off value or 0.05%, whichever was higher (responses below this cut-off were considered negative or to have a response = 0). For this study, the net responses to the ten Mtb Ags in blood in all the quantiferon-negative RM pre-vaccination, was determined to be 0.004% ± 0.004% for CD4⁺ T cells (cut-off = 0.02%) and 0.003% ± 0.004% for CD8⁺ T cell responses (cut-off = 0.02%). For BAL, the mean background ± s.d. was determined to be 0.004% ± 0.008% for both CD4⁺ and CD8⁺ T cells (cut-off = 0.036%). Because these cut-off levels were all <0.05%, we used our conservative default cut-off of 0.05% for all responses. For memory phenotype and polycytokine analysis of Mtb-Ag-specific T cells, all cells expressing CD69 plus one or more cytokines were first Boolean-gated, and then this overall Ag-responding population was subdivided into the subsets of interest on the basis of surface phenotype or cytokine production pattern^{22,23}.

A customized Luminex subclass assay⁶³ was used to quantify the relative concentration of each immunoglobulin (Ig) isotype among the Mtb-antigen-specific Abs. Carboxylated microspheres (Luminex) were coupled with Mtb protein Ags by covalent *N*-hydroxysuccinimide (NHS)-ester linkages via the cross-linker EDC and NHS (Thermo Scientific) per the manufacturer's instructions. Ag-coated microspheres (5,000 per well) were added to a 96-well filter plate (Millipore). Each Ig sample (5 μg) was added to five replicate

wells of a 96-well plate and incubated for 16 h at 4 °C. The microspheres were washed, and the Ig-isotype-specific detection reagents were added (Southern Biotech) for 2 h at room temperature. The beads were then washed and read on a Bio-Plex 200 System. The background signal, defined as mean fluorescence intensity (MFI) of microspheres incubated with PBS, was subtracted. Each sample was tested twice.

Mycobacterial (Mtb) culture. Tissues routinely collected at necropsy for Mtb burden analysis in both Study 1 and Study 2 included: 30 stereologic punches from right-lung lobes, ten punches from left-lung lobes, trachea, left hilar LN, right hilar LN, left carinal LN, right carinal LN, paratracheal LN, mediastinal LN, axillary LN, inguinal LN, mesenteric LN, spleen, pancreas, left medial lobe of liver, right medial lobe of liver, left lateral lobe of liver, right lateral lobe of liver, liver caudate, left kidney and right kidney. In Study 2 we also collected and cultured the retropharyngeal LN, tonsil, submandibular LN and iliosacral LN. In one RM in Study 2, Mtb culture analysis was not reported due to gross contamination of thoracic tissues with granuloma contents. Tissues were collected in Hank's balanced salt solution (HBSS; Hyclone, SH30031.03) and were then homogenized in an IKA grinder tube with an IKA Ultra-Turrax Tube Drive homogenizer. The tissue homogenate was then filtered over a 70- μ m wire screen to remove debris, and 200 μ l of this material was plated neat and in serial dilutions (1/10 and 1/100) on 7H11 agar plates (Remel). All plates were incubated at 37 °C, and *M. tuberculosis* growth was enumerated 28 and 42 d later. A tissue was considered Mtb⁺ if any colonies with the correct morphologic features were identified. Selected cultures were analyzed by the Ziehl–Neelsen method for acid-fast bacteria to confirm colony morphology. Bacterial density in lung-draining LNs was calculated in CFUs per gram of tissue.

Data preparation (immunology and vaccine-mediated protection). *Area under the curve of log(CT-scan-determined pulmonary disease volume).* We computed the AUC of the log-transformed CT-scan-determined pulmonary disease volume measurements from time 0 (set to 0) to day 112. Next, we imputed missing values for monkeys that were taken to necropsy before the full series of scheduled CT scan time points. We computed the AUC of this augmented data. The imputation procedure that we employed used linear regression to estimate missing values from previous time points. As a sensitivity analysis, we also imputed the missing values using a more conservative rule (replacing missing values with the largest non-missing value at the same time point among monkeys receiving the same treatment, excluding for further conservatism one high-valued outlier unvaccinated RM); the resulting AUCs were highly insensitive to this procedure (Pearson correlation >0.99 for both studies).

Necropsy score data. The non-negative count-valued necropsy scores were amenable to Poisson modeling. Model evaluations supported inclusion of the additional parameter for overdispersion in the negative binomial model. In TB Study 2, the estimated extra parameter was zero, so this model was equivalent to a simple Poisson model. For this Poisson modeling we used sandwich-based estimates of variance–covariance matrices as an alternative method to account for overdispersion, using the `vcovHC` function in the sandwich package in R^{63–65}. We also considered and rejected using the zero-inflated Poisson (ZIP) model.

Necropsy culture data. Necropsy culture inputs were quantitative measures of culture growth with multiple replicates per tissue. We treated these data as binary indicators of a culture being positive versus negative (zero) and evaluated the total number of positive cultures. Model evaluations of necropsy culture outcome data favored the more expressive negative binomial models over Poisson models and did not support using the ZIP model. Note that one animal in TB Study 2 (I3; see **Supplementary Fig. 9**) was missing necropsy culture data but did have necropsy score data; the analyses of the culture data therefore excluded this RM. Thus, for the left panels in **Figure 4f–h** ('positive Mtb cultures'), the sample size for the 68-1.2-9Ag (green-colored) group was $n = 8$. As described below, we imputed the missing value for use in computing the scaled (normalized) combination outcome measure.

Scaled (normalized) combination outcome measure. As shown in **Supplementary Figure 5**, we found a strong correlation between the necropsy score and necropsy culture outcome measures within each study, although the scales were different—necropsy cultures were about one-third as large as necropsy scores in both studies. We created the intermediate,

study-specific scaled combination outcome measure to gain measurement precision by averaging these two very similar outcome measures. To ensure that each receives equal weight in the combined measure, and to maintain discreteness in support of Poisson analysis of the statistic, we first scaled the inputs by multiplying the necropsy culture values by 3 and then adding these to the necropsy scores. For Study 2, as indicated above, one RM (I3) had a missing necropsy culture value, so for this animal we computed the scaled combination outcome measure using an imputed necropsy culture value, which we obtained by multiplying the observed necropsy score value by the estimated coefficient from a simple linear regression model relating the two values. This monkey's necropsy score value was 29, its imputed necropsy culture value was 8, and its scaled combination outcome measure value was 53. We used a negative binomial regression model of these study-specific combined measures versus treatment and study, and used the estimated coefficient on study (0.3796) to further scale the TB Study 1-scaled combination outcome values. Therefore, the scaled combination outcome variable for TB Study 1 RMs is the study-specific value multiplied by 0.3796, which was then rounded to maintain the discreteness of the final variable for Poisson analysis.

Challenge-phase LN Mtb cell-forming units per gram. We computed the mean of log₁₀-transformed measures of Mtb CFUs per gram across five LN tissue samples (carinal left and right, hilar left and right, and paratracheal). The few missing values were first imputed using the mean value for the LN.

End-of-vaccine-phase T cell response data. We also evaluated longitudinal flow cytometric ICS measures of CD4⁺ and CD8⁺ immune responses that targeted the nine individual Mtb proteins in the RhCMV vaccines, and CFP-10. Our primary summary of these data was a measure of the immune response at the end of the vaccination phase. These pre-challenge baseline immunogenicity values were the geometric means of three independent measurements over the time periods shown in **Figures 1a and 3a**. Totals for the six or nine antigens were computed before log-transformation and normalization. Normalization shifts and scales these values to have a mean value of zero and an s.d. of 1, so that units have the interpretation of z-scores that measure the number of s.d. that an immune measurement (on the log scale) is from the overall (study-specific) mean of that measurement.

Change-from-baseline T cell responses after Mtb challenge. We computed AUC values of time-varying differences from the pre-challenge baseline immunogenicity values for each of the nine insert antigens over 42 d or 98 d post challenge (for TB Study 1 and Study 2, respectively), on the natural (pre-log-transformation and pre-normalization) scale.

Antibody responses to vaccination. We computed log₁₀-transformed baseline-subtracted MFI values after replacing differences of <1 by 1 (such that after log₁₀ transformation these values are zero). For plotting purposes, we computed positivity thresholds as the median among unvaccinated RMs of the baseline-subtracted measure before truncation and log transformation, plus three s.d. For TB antigens, we computed these threshold values separately for Study 1 and Study 2. For the SIV gp120 control Ag, which was used as a positive control using Ig obtained from five SIV-infected RMs (SIVIg), we computed this background threshold using the unvaccinated RMs from both of the studies (these values were plotted along with the SIVIg values in the inset of **Supplementary Fig. 1b**).

Statistical analysis (immunology and vaccine-mediated protection). All statistical analyses were conducted in R⁶⁴ (also, see the **Life Sciences Reporting Summary**).

Sample size and treatment assignment. For both studies, the primary constraint on sample size was the availability of RM subjects and BSL-3 facilities. Groups were balanced for monkey traits and treatments were assigned nonrandomly but arbitrarily.

Vaccine-mediated protection. As described above, we evaluated three primary outcome measures for evidence of a difference across treatment arms within each study: CT scan AUC from challenge to day 112 post challenge, pathologic score at necropsy and extent of Mtb infection at necropsy (number of Mtb⁺ tissues). The equivalence of the three Study 2 vaccine groups by these outcome measures (**Supplementary Fig. 4**) justified a pooled analysis. We employed nonparametric tests for primary comparisons and used parametric models for

estimating confidence intervals of treatment effects. For comparisons of outcome measures across pairs of groups, we used two-sided Wilcoxon tests. Box plots in **Figures 2** and **4** show unadjusted P values of only the pairwise comparisons that are significant at the 0.05 level. We employed Holm adjustment⁶⁶ for the specified primary nonparametric comparisons: between unvaccinated and vaccinated TB Study 1 groups, and separately between BCG-only and other vaccinated groups. For TB Study 2, we similarly applied a Holm adjustment within groups of comparisons between unvaccinated and vaccinated TB Study 2 groups individually, and between the RMs administered the original 68-1-9Ag vector and those given modified vectors (68-1-6Ag and 68-1.2-9Ag). Box plots show unadjusted P values; Holm-adjusted P values are shown in **Supplementary Figure 4**. Vaccine-mediated protection is reported as $100\% - W$, where W is $100 \times$ the estimated rate (or confidence limit) of the Poisson or negative binomial model representing a count-valued outcome measure (necropsy score, necropsy culture or the scaled combination outcome measure) among a vaccine group, as a fraction of the rate for unvaccinated RMs. For analysis of correlations across outcome variables, we used Spearman's rank-transformed correlation statistic (r) and test. For the Spearman's test, P values were computed via the asymptotic t approximation using the 'cor.test' method in R. Binary comparisons of the dichotomous end point defined by any evidence of TB disease at necropsy were conducted using Fisher's exact test, and confidence intervals for the dichotomous end point were estimated using Wilson's score method⁶⁷.

T cell and antibody immunogenicity and immune correlates analysis. For comparisons of T cell immunogenicity across vaccine-receiving treatment groups at pre-challenge baseline, for comparisons of changes from baseline after challenge and for comparisons of pre-challenge Ab responses across treatment groups, we first used Kruskal–Wallis (KW) tests. For panels with a KW test unadjusted $P \leq 0.05$, the box plots indicate significance of pairwise Wilcoxon tests that had a Holm-adjusted $P \leq 0.05$. Due to the lack of blood immunology data from week 41 of RM U6 (Study 1; BCG-only group), for **Figure 1d**, the BCG group had an $n = 6$, and for **Figure 1c**, the data point for this RM used only two, rather than three, time points to obtain an average. Due to the lack of immunology data of RMs D1 and D2 (Study 1; unvaccinated group), the unvaccinated group had an $n = 6$. For analysis of immune response correlations with the scaled combination outcome measure (defined above) among the RMs that received the RhCMV vector and no BCG, we computed Spearman's statistic and test, and in the scatter plots we also show the curve of the best-fitting negative binomial model. We confirmed through sensitivity analyses that the low correlations (**Supplementary Fig. 10**) were also found in each study separately and in each outcome measure, so the lack of significance was not an artifact of these analysis choices. Extensive nonparametric analyses, as well as parametric analyses, employing negative binomial models to estimate single-parameter and multiparameter associations between this scaled combination measure and pre-challenge immune responses to RhCMV immunogens revealed no statistically supported ICS-determined T cell response magnitude correlate of that outcome, or of other related outcomes.

Transcriptomic analysis. RNA processing and sequencing. Whole blood was drawn from the RMs directly into PAXgene blood RNA tubes (PreAnalytiX, Hombrechtikon, Switzerland), which were stored at -20°C . RNA was extracted from the blood in the PAXgene tubes according to the manufacturer's instructions. Depletion of globin transcripts (GlobinClear, ThermoFisher Scientific, MA, USA) was performed on the extracted RNA, followed by cDNA library preparation using the Illumina TruSeq Stranded mRNA Sample Preparation Kit (Illumina, CA, USA) for Study 1, and Eukaryote Transcriptome Library Construction Protocol (SOP-TRA J005, Beijing Genomics Institute, Shenzhen, China) for Study 2. For Study 1, globin transcript depletion, cDNA library preparation and RNA sequencing were performed by Expression Analysis/Q2 Solutions, Inc. (Durham, NC). For Study 2, these services were provided by Beijing Genomics Institute (Shenzhen, China). For Study 1, the sequencing strategy was 51-bp paired-end reads at an average sequencing depth of 40 million reads per sample. For Study 2, the sequencing strategy was 49-bp paired-end reads at an average sequencing depth of 70M reads per sample. RNA extraction failure for one RM from the Study 1 BCG group (U2), one RM of the Study 1 68-1 RhCMV/TB group (N1) and four RMs from the

unvaccinated group (L1, L2, D1 and D2) precluded generation of RNA-seq data for these animals, giving a total of 23 RMs that were analyzed by RNA-seq for Study 1 ($n = 4$ for unvaccinated; $n = 6$ for RhCMV/TB vaccinated; $n = 6$ for BCG vaccinated; $n = 7$ for BCG + RhCMV/TB vaccinated). All 36 Study 2 RMs were analyzed by RNA-seq ($n = 9$ for each group). For Study 1, RNA samples collected on the day of challenge and at 14 d and 28 d after challenge were analyzed by RNA-seq. For Study 2, RNA samples that were collected before vaccination (for the RhCMV/TB-vaccinated groups), on the day of challenge and at 28 d after challenge were analyzed by RNA-seq.

RNA-seq data processing. Read pairs were preprocessed using scripts that adjusted base calls with phred scores < 5 to 'N' and removed read pairs for which either end had fewer than 30 unambiguous (non-N) base calls. Processed read pairs were aligned using STAR (v.2.3.0.1)⁶⁸ to the MacaM assembly⁶⁹. Read pairs in which both ends mapped concordantly were used as input to the HTSeq program⁷⁰ (run in stranded, intersection-strict mode) to assign gene counts. Of the 16,050 gene models, 11,977 and 12,517 had at least 10 counts in at least 5% of the samples from Study 1 and Study 2, respectively, with 11,678 gene models meeting these criteria in both studies. Log_2 -transformed values of counts normalized by trimmed mean of M-values (TMM)⁷¹ adjusted library counts were computed for Study 1 and Study 2 using the 'calcNormFactors' function of the edgeR package⁷² and the 'voom' function of the package limma⁷³. This widely applied transformation was sought to normalize estimated gene expression levels for differences in both library size and overall transcriptome diversity and was expected to help minimize the effect of technical differences between samples or protocols between Study 1 and Study 2.

Log_2 -transformed counts for Study 1 and Study 2 were then merged into a unified data set that was used for all subsequent RNA-seq-based correlates analyses.

Identification of commonly regulated genes in patients with TB and in unvaccinated RMs from Study 1 and Study 2 after Mtb challenge. Normalized Illumina microarray data for HIV-uninfected South African and Malawi patients with TB ($n = 46$ from South Africa; $n = 51$ from Malawi) or control individuals with latent TB infection (LTBI) ($n = 48$ from South Africa; $n = 35$ from Malawi) from a previously published human TB study³⁷ was downloaded from the Gene Expression Omnibus along with the Entrez Gene annotations for the microarray platform. For cases in which multiple probes targeted a common gene, the probe with the maximum 90% quantile of gene expression was selected. The human microarray and macaque RNA-seq data sets were then matched in terms of gene symbols, yielding 10,075 genes that were assayed by both platforms. TB-associated genes in the human study were identified by two-sided Wilcoxon tests comparing the patients with TB to control individuals for the South African and Malawi sites. For each gene, the maximum Wilcoxon P value for the two sites was FDR-adjusted for multiple comparisons using the Benjamini–Hochberg FDR adjustment procedure, after having first assigned $P = 1$ for any genes with discordant patterns between the cohorts. The purpose of using the maximum P value from the two sites as a summary statistic was to ensure that only genes were selected that were robustly and consistently associated with TB disease, irrespective of any site-associated contributions of genetics or environment to transcriptional levels. At a significance threshold of $P < 0.05$ and $\text{FDR} < 0.33$, 3,406 TB-responsive genes were identified from the human study. These genes were then tested for responses in the unvaccinated RMs from Study 1 ($n = 4$) and Study 2 ($n = 9$) by one-sided paired Wilcoxon tests comparing expression at 28 d after challenge to pre-challenge levels, using the directionality from the response in humans. At a significance threshold of $P < 0.05$ and $\text{FDR} < 0.33$, 1,482/3,406 TB-responsive genes from the human study were validated in the RM model, and median fold changes were correlated between both systems (**Fig. 5a,b** and **Supplementary Table 1**).

Identification of associations between transcriptional responses and outcome. Poisson regression modeling with sandwich adjustment, as described above (necropsy score data), was used to test whether expression levels or fold changes in expression were significant predictors for outcome after challenge, as indicated by the scaled combination outcome measure. Briefly, Wald tests (R function: waldtest()); library: lmtree⁷⁴ with the regression coefficient covariance matrix being provided by heteroskedasticity-consistent covariance matrix estimation (R function: vcovHC(), library: sandwich^{63,64}) were performed comparing two Poisson regression models that were generated for each gene:

Model 1: outcome ~gene + Study

Model 2: outcome ~Study

where 'outcome' indicates the scaled combination outcome measure, 'gene' indicates the \log_2 -transformed expression level or fold change in expression for a specific gene, and 'Study' indicates an additive factor with two levels: 0 or 1, with '0' corresponding to Study 1, and '1' corresponding to Study 2.

Although the scaled combination outcome measure is harmonized between Study 1 and Study 2, minor technical differences in the RNA-seq analysis between Study 1 and Study 2 (for example, sequencing depth, library protocol or service provider) may give rise to small shifts in expression between Study 1 and Study 2 that could confound the modeling; including the additive 'Study' term in the model addresses this possible effect. Wald test P values from comparing model 1 with model 2 were FDR-adjusted for multiple comparisons using the Benjamini–Hochberg procedure. This overall strategy was applied to identify the post-challenge (Fig. 5) and pre-challenge (Fig. 6) transcriptional correlates with outcome as described below:

Post-challenge correlates with outcome. When modeling outcome as a function of the \log_2 (fold change in expression post challenge (i.e., day 28/day of challenge)), data from all of the RMs were included (all RhCMV/TB groups, and BCG and unvaccinated groups; $n = 59$) from Study 1 and Study 2. To focus the analysis on the TB disease signature that is common between humans and RMs, the set of genes analyzed was restricted to the 1,482 TB-responsive genes that were discovered in the human TB cohort and validated in the unvaccinated RM (Fig. 5a). At the thresholds applied in the other analyses ($P < 0.05$ and FDR < 0.33), a large number of significant associations were detected (1,007 genes). For this reason, an additional filtering step was applied to focus the results on the strongest associations. Requiring that the absolute value of the overall Kendall tau rank correlation coefficient between the scaled combination outcome measure and gene expression fold changes exceed a value of 0.4 yielded the final set of 214 genes shown in Fig. 5c (Supplementary Table 3).

Pre-challenge correlates with outcome. When modeling outcome as a function of the \log_2 (expression levels measured immediately before challenge), two analyses were performed: (i) using data from all RMs that received RhCMV/TB vaccines (all RhCMV/TB groups and the BCG + RhCMV/TB group from Study 1; $n = 40$), and (ii) using data from the unvaccinated and BCG (only) vaccine groups ($n = 19$; Fig. 6a–c). The objective of the former was to identify pre-challenge correlates of eventual protection or susceptibility that were operational within the context of RhCMV/TB-induced immune responses (note that RhCMV/TB-elicited Mtb-specific T cell responses were similar regardless of prior BCG vaccination; Fig. 1b–f), whereas the objective of the latter was to confirm that the associations in (i) were restricted to the context of RhCMV/TB vaccination and less likely to be due to monkey-intrinsic differences. Prior to Poisson regression analysis, the average pre-challenge \log_2 -transformed expression levels for the unvaccinated RM was subtracted from the pre-challenge \log_2 -transformed expression levels of all RM within the same study.

For the RhCMV/TB-focused analysis (i), the complete transcriptome (11,678 genes) was analyzed. At the thresholds applied in the other analyses ($P < 0.05$ and FDR < 0.33), 475 genes with significant associations were identified. This initial set was reduced to 315 genes by requiring that the sign of the Kendall tau rank correlation coefficient between gene expression and outcome be consistent for Study 1 and Study 2 (different correlation signs could arise from the difference in sample numbers between Study 1 and Study 2; requiring consistent directionality penalized associations driven predominantly by Study 2 in favor of shared associations). We noted that genes with overall negative correlations with outcome exhibited much greater sign consistency between Study 1 and Study 2 than genes with overall positive correlations with outcome (94/107 consistent genes negatively correlated with outcome; 221/368 consistent genes positively correlated with outcome). The genes with the strongest associations between \log_2 (expression) and outcome were then identified by ranking the absolute value of the overall Kendall tau rank-correlation coefficient between the scaled combination outcome measure and \log_2 (gene expression levels) (using 'study-adjusted' values for genes with nominally significant study terms, as defined below). Requiring the absolute value of the Kendall tau coefficient to exceed 0.2 yielded a set of 280 genes for subsequent analysis. All arbitrary thresholds including this Kendall tau threshold were determined

once and held fixed thereafter to ensure interpretability of resulting statistics. To determine whether these candidate signatures were potentially driven by the RhCMV/TB vaccine, we tested whether these genes exhibited significant associations with outcome for the BCG and unvaccinated groups by Poisson modeling as described above. Of the 280 genes, seven were nominally significant ($P < 0.05$), and 22 exhibited $P < 0.2$, indicating an overall absence of evidence for an association between the expression of the gene set and outcome for RMs that did not receive RhCMV/TB vaccination. The 22 genes with $P < 0.2$ for analysis (ii) were excluded, yielding the 258 genes shown in Figure 6a (Supplementary Table 5). Of these, 181 exhibited pre-challenge expression levels that were positively correlated with values of the scaled combination outcome measure and were termed the 'susceptibility signature', meaning that higher expression of these genes before Mtb exposure was associated with a tendency to ultimately develop more severe disease. Seventy-seven of the 258 genes exhibited pre-challenge expression levels that were negatively correlated with values of the scaled combination outcome measure and were termed the 'protection signature', meaning that higher expression of these genes before Mtb exposure was associated with a tendency to ultimately develop less severe disease or even to have complete protection.

As described in the Results, inspection of the heat map visualizations of protection and susceptibility signatures (Fig. 6a,b) suggested that the association between pre-challenge expression levels and outcome was predominantly binary, with strongly protected RMs exhibiting a distinct expression pattern as compared to that in all of the other RMs. This conjecture was explored by logistic regression modeling in which the scaled combination outcome measure was discretized into two levels: 'completely protected' (14 RMs that exhibited no signs of disease) and 'non-protected' (all other RMs that received RhCMV/TB vaccine). The modeling was essentially done as described above, replacing non-negative discrete numeric 'outcome' with binary 'protection', and employing Chi-squared tests to compare models in lieu of the Wald test. Also, instead of performing the modeling by including a 'Study' term (model 1 and model 2), the 'Study' term was removed, and the modeling was performed using the study-adjusted expression values for instances where the 'Study' term was statistically significant based on the full Poisson models (model 1 and model 2). This is because there was only one protected RM in Study 1, and it is therefore not possible to reliably estimate a 'Study' term for the logistic regression models. In addition to evaluating the statistical significance of the binary models, discriminatory potential of the models was evaluated using receiver operating curve (ROC) metrics (R package: pROC) to assess ROC AUC values and stratified accuracy for Study 1 and Study 2 at the optimal ROC operating point. As described, results of this analysis supported the binary interpretation of the signatures, with 49% and 39% of protection and susceptibility genes, respectively, exhibiting 'reasonable discriminatory ability' (Supplementary Table 5), which we defined as $P < 0.05$, ROC AUC lower 95% confidence interval > 0.5 , and having a ROC operating point that simultaneously achieves at least 50% sensitivity and specificity in both Study 1 and Study 2.

Heat map visualizations. Heat map visualizations were generated in R using the 'pheatmap' library.

Post-challenge correlates with outcome. The 'Study' term in model 1 was not nominally significant for any of the 214 genes identified (i.e., $P > 0.05$), and for this reason, the \log_2 (fold change) data shown in Figure 5c–e are presented without any additional transformations beyond the overall scaling for the heat maps (dividing the values for each gene by the maximum absolute fold change in expression observed for that gene).

Pre-challenge correlates with outcome. The 'Study' term in model 1 was nominally significant for about half of the genes identified, indicating small differences in pre-challenge gene expression that did not influence associations with outcome but that did complicate visualizations. For these genes, study-adjusted \log_2 -transformed expression profiles were computed by adding to Study 2 \log_2 -transformed expression levels the estimate of the 'Study' coefficient divided by the estimate of the 'gene' coefficient from model 1. This transformation aligned the Study 1 and Study 2 \log_2 expression levels to a common trajectory and facilitated visualization of the associations with outcome identified by the modeling. In the heat maps, \log_2 expression profiles or study-adjusted \log_2 expression profiles are shown after scaling the values for each gene by the maximum absolute fold change in expression observed for that gene.

Module and pathway enrichment analysis. Fisher's exact test was employed to determine whether genes belonging to pre-defined transcriptional modules or immune pathways were significantly over-represented within sets of genes that were identified as associated with outcome or other characteristics. This analysis used two external sources for association of specific genes with transcriptional modules or pathways. The first was the set of blood transcriptional co-expression modules defined by Obermoser, *et al.*⁵³. These modules are advantageous because they define sets of similarly annotated genes that exhibit concordant expression patterns across an extensive set of immune-related transcriptional profiles from blood. Enrichment analysis of these modules was restricted to the annotated modules, and modules with common annotations were merged. Definition and annotation of the modules is provided at http://www.biir.net/public_wikis/module_annotation/G2_Trial_8_Modules. The transcriptional modules were complemented by curated pathway definitions from Reactome⁵⁴, which are not based on co-expression but rather on extensive signaling pathway knowledge from the literature. Enrichment analysis of these pathways was restricted to those within the 'immune system' branch of the overall hierarchy. Each enrichment analysis required a 'reference' gene set that constituted the relevant compendium of candidate genes from which the gene set of interest was derived. The reference gene sets for each enrichment analysis are defined below. To exclude spurious enrichment results, modules and pathways with fewer than 50 members within the reference gene set were excluded. Gene sets for enrichment analysis were defined according to the association of interest and directionality (i.e., upregulated genes were tested for module and pathway over-representation separately from downregulated genes). Multiple comparisons were addressed by performing the Benjamini-Hochberg adjustment to the Fisher's exact test *P* values, with *P* values for gene sets derived from a common analysis, but exhibiting opposite directionality, being adjusted together. Enrichment significance thresholds were set at *P* < 0.05 and FDR < 0.15.

Enrichment analysis of TB-responsive genes in humans and RMs (Fig. 5b and Supplementary Table 2). The reference gene sets were the 10,075 genes commonly detected in the human and NHP platforms, and the gene sets of interest were the 793 upregulated and 689 downregulated genes from the 1,482 genes regulated in common. Enriched modules and pathways with fewer than 20 members within the upregulated and downregulated genes are not shown.

Enrichment analysis of TB-responsive genes with post-challenge fold changes in expression associated with outcome (Fig. 5c,d and Supplementary Table 4). The reference gene sets were the 1,482 genes that were regulated in common between humans and NHPs, and the gene sets of interest were the 196 genes that were positively associated, and 18 genes that were negatively associated with outcome (from the 214 with post-challenge fold-changes associated with outcome). Enriched modules and pathways with fewer than two members within the positively and negatively associated genes are not shown.

Enrichment analysis of genes with pre-challenge expression profiles that are associated with outcome in RhCMV/TB-vaccinated RMs (Fig. 6a,b and Supplementary Table 8). The reference gene sets were the 11,678 genes detected in common between Study 1 and Study 2, and the gene sets of interest were the 181 genes positively associated (susceptibility signature) and 77 genes negatively associated (protection signature) from the 258 with pre-challenge expression profiles associated with outcome. Enriched modules and pathways with <2 members within the positively and negatively associated genes are not shown.

Integration of transcriptional measurements with leukocyte population counts. To gain insight into the contribution of leukocyte trafficking to the pre-challenge protection and susceptibility signatures, we integrated the transcriptome data with whole-blood leukocyte percentages. Bulk lymphocyte, monocyte and neutrophil population percentages in whole blood on the day of challenge were determined by a Coulter counter (Study 1) and a Horiba blood cell counter (Study 2). Basophil and eosinophil counts were excluded because they were marginal in both studies and were not likely to contribute to the whole-blood transcriptome readouts. The contribution of T cells (CD3⁺) and T cell subsets (CD4⁺ and CD8⁺) to the bulk lymphocyte count was further determined for Study 1 and Study 2 by flow cytometry. Leukocyte counts were used in three exploratory analyses: (i) testing leukocyte populations themselves for pre-challenge associations with outcome, (ii) identifying the leukocyte population

most associated with specific genes and (iii) determining whether leukocyte population differences may have been responsible for the pre-challenge transcriptional associations with outcome. Both untransformed and log₁₀-transformed leukocyte percentages were investigated in the exploratory analyses.

Testing leukocyte populations alone for pre-challenge associations with outcome. In this analysis, the Poisson regression analysis (described above) for identifying pre-challenge transcriptional correlates with outcome was repeated exactly, but with the substitution of leukocyte population counts (and log transformations thereof) instead of genes. No single leukocyte population, nor ratios between monocytes and lymphocytes, neutrophils to lymphocytes, or neutrophils to monocytes, achieved nominally significant associations with outcome (i.e., *P* > 0.05 for all populations) or nominally significant Kendall rank correlations with outcome (i.e., *P* > 0.05 for all populations).

Identification of the leukocyte population most associated with specific genes. Given the nontransitive nature of correlations, it was possible that genes that were significantly associated with outcome may have been significantly associated with certain leukocyte populations, even if those leukocyte populations themselves were not significantly associated with outcome. This scenario could arise, for example, if the activation state of a certain leukocyte subpopulation, as indicated by expression of a specific gene set, was associated with outcome. We determined the leukocyte population associated with each gene by performing robust linear regression (R: rlm, package: MASS) using the following model structure:

Model 3: $Cell \sim gene + Study$

where Cell indicates the leukocyte population percentage of interest (neutrophils, monocytes, lymphocytes, T cells, CD4⁺ T cells or CD8⁺ T cells, and the log transformations thereof), and 'gene' and 'Study' are defined as for models 1 and 2.

Because the focus of the analysis was for the interpretation of the pre-challenge protection and susceptibility signatures (Fig. 6a), robust linear regression modeling was restricted to leukocyte counts and transcriptome data for RMs that received RhCMV/TB vaccinations. The significance of the association between the gene and leukocyte population was determined by robust *F*-tests on the 'gene' coefficient from the model (R: frobtest, package: sfsmisc). Plausible leukocyte/cell associations were defined as those for which the model coefficient was nominally significant (*P* < 0.05) and the coefficient was positive (indicating a positive relationship between transcription and the cells). Of the genes with more than one plausible association that met these criteria, the cell population with the smallest *P* value was selected.

To determine whether genes with plausible associations with specific leukocyte populations were over-represented in the pre-challenge protection or susceptibility signatures, Fisher's exact tests were performed as described above, except for replacing the transcriptional module and pathway annotations with the associations between genes and cell populations. Given the hierarchical relationship between CD4⁺ and CD8⁺ T cells, T cells and lymphocytes, genes and lymphocyte associations detected lower in the hierarchy were also assigned to upper branches of the hierarchy (i.e., a gene associated with CD4⁺ T cells would also be counted as a gene associated with T cells and lymphocytes). Similarly, genes that were most associated with actual CD4⁺ T cell percentages or log-transformed CD4⁺ T cell percentages were simply regarded as 'CD4⁺ T cell associated'. The full list of gene by leukocyte populations is provided in **Supplementary Table 6**. Enrichment results for association with leukocyte populations are provided in **Supplementary Table 7**.

Determining whether leukocyte population differences may be responsible for the pre-challenge transcriptional associations with outcome. Additional Poisson regression analyses were performed to determine whether the association between pre-challenge expression of a certain gene and outcome were driven by the leukocyte population with which the gene was most associated. This followed the identical sandwich-adjusted Poisson modeling and Wald test for model comparison as described above, except for the inclusion of new terms for the leukocyte population associated with the gene being tested:

Model 4: $outcome \sim gene + Cell + Study$

Model 5: $outcome \sim Cell + Study$

where Cell indicates the leukocyte population most associated with the gene being analyzed, and 'gene' and 'Study' are as defined earlier.

If variation in the leukocyte population was driving the association between outcome and the gene, then the gene would not contribute to the model fit and there would be no statistically significant difference revealed by the Wald test comparing model 4 and model 5. As described above, this analysis was performed only for RMs that received the RhCMV/TB vaccine, only at the pre-challenge time point, and only for those genes from the protection and susceptibility signatures (Fig. 6a) for which there was a plausibly associated leukocyte population. Of the 280 genes, 82 were associated with at least one leukocyte population, and four of these (*AMIGO1*, *DDX39B*, *GMEB2* and *TYSND1*; all from the susceptibility signature) lost nominal significance in the comparison between models 4 and 5 (*P* values ranged from 0.05 to 0.08 for these genes) (Supplementary Table 5). This result suggests that the protection and susceptibility signatures do not likely result from, nor are driven by, trafficking differences in bulk leukocyte populations.

Testing for differences between RhCMV/TB and BCG + RhCMV/TB pre-challenge transcriptional patterns. One-sided Wilcoxon rank-sum tests were performed to compare the expression levels of genes from the protection signature in the RhCMV/TB group (*n* = 6) to the BCG + RhCMV/TB (*n* = 7) group from Study 1. Given the tendency within the BCG + RhCMV/TB group toward reduced protection, we tested whether pre-challenge expression of the protection-associated genes was reduced in this group as compared to that in the group that received RhCMV alone. At *P* < 0.05 and FDR < 0.33, 15 genes were identified that met this criterion (Fig. 6d and Supplementary Table 9).

Life Sciences Reporting Summary. Further information on experimental design is available in the **Life Sciences Reporting Summary**.

Data availability. The data sets generated and/or analyzed during the current study, as well as the computer code used to perform statistical analysis, are available from the corresponding authors on reasonable request. Raw and processed RNA-seq data for Study 1 and Study 2 have been deposited into the Gene Expression Omnibus under accession code [GSE102440](https://www.ncbi.nlm.nih.gov/geo/query/acc.cgi?acc=GSE102440).

57. National Research Council. *Guide for the Care and Use of Laboratory Animals* 8th edn. (The National Academies Press, 2011).
58. Capuano, S.V. III *et al.* Experimental *Mycobacterium tuberculosis* infection of cynomolgus macaques closely resembles the various manifestations of human *M. tuberculosis* infection. *Infect. Immun.* **71**, 5831–5844 (2003).
59. Rumboldt, Z., Huda, W. & All, J.W. Review of portable CT with assessment of a dedicated head CT scanner. *AJNR Am. J. Neuroradiol.* **30**, 1630–1636 (2009).
60. Rubin, G.D. Lung nodule and cancer detection in computed tomography screening. *J. Thorac. Imaging* **30**, 130–138 (2015).
61. Luciw, P.A. *et al.* Stereological analysis of bacterial load and lung lesions in nonhuman primates (rhesus macaques) experimentally infected with *Mycobacterium tuberculosis*. *Am. J. Physiol. Lung Cell. Mol. Physiol.* **301**, L731–L738 (2011).
62. Zvi, A., Ariel, N., Fulkerson, J., Sadoff, J.C. & Shafferman, A. Whole-genome identification of *Mycobacterium tuberculosis* vaccine candidates by comprehensive data mining and bioinformatic analyses. *BMC Med. Genomics* **1**, 18 (2008).
63. Zeileis, A. Object-oriented computation of sandwich estimators. *J. Stat. Softw.* **16**, 1–16 (2006).
64. Zeileis, A. Econometric computing with HC and HAC covariance matrix estimators. *J. Stat. Softw.* **11**, 1–17 (2004).
65. R Core Team. *R: A Language and Environment for Statistical Computing* (R Foundation for Statistical Computing, 2015).
66. Holm, S. A simple sequentially rejective multiple-test procedure. *Scand. J. Stat.* **6**, 65–70 (1979).
67. Agresti, A. & Coull, B.A. Approximate is better than “exact” for interval estimation of binomial proportions. *Am. Stat.* **52**, 119–126 (1998).
68. Dobin, A. *et al.* STAR: ultrafast universal RNA-seq aligner. *Bioinformatics* **29**, 15–21 (2013).
69. Zimin, A.V. *et al.* A new rhesus macaque assembly and annotation for next-generation sequencing analyses. *Biol. Direct* **9**, 20 (2014).
70. Anders, S., Pyl, P.T. & Huber, W. HTSeq—a Python framework to work with high-throughput sequencing data. *Bioinformatics* **31**, 166–169 (2015).
71. Robinson, M.D. & Oshlack, A. A scaling normalization method for differential expression analysis of RNA-seq data. *Genome Biol.* **11**, R25 (2010).
72. Robinson, M.D., McCarthy, D.J. & Smyth, G.K. edgeR: a Bioconductor package for differential expression analysis of digital gene expression data. *Bioinformatics* **26**, 139–140 (2010).
73. Ritchie, M.E. *et al.* limma powers differential expression analyses for RNA sequencing and microarray studies. *Nucleic Acids Res.* **43**, e47 (2015).
74. Zeileis, A. & Hothorn, T. Diagnostic checking in regression relationships. *R News* **2**, 7–10 (2002).

Life Sciences Reporting Summary

Nature Research wishes to improve the reproducibility of the work that we publish. This form is intended for publication with all accepted life science papers and provides structure for consistency and transparency in reporting. Every life science submission will use this form; some list items might not apply to an individual manuscript, but all fields must be completed for clarity.

For further information on the points included in this form, see [Reporting Life Sciences Research](#). For further information on Nature Research policies, including our [data availability policy](#), see [Authors & Referees](#) and the [Editorial Policy Checklist](#).

Please do not complete any field with "not applicable" or n/a. Refer to the help text for what text to use if an item is not relevant to your study. For final submission: please carefully check your responses for accuracy; you will not be able to make changes later.

▶ Experimental design

1. Sample size

Describe how sample size was determined.

No statistical methods were used to predetermine sample sizes.

2. Data exclusions

Describe any data exclusions.

Criteria for when to take monkeys to necropsy were pre-established. No data were excluded from these analyses. Missing data were imputed where the imputation was shown to be robust, as described in Methods.

3. Replication

Describe the measures taken to verify the reproducibility of the experimental findings.

A second vaccine study was performed and this second study reproduced the primary efficacy estimates of RhCMV/TB versus unvaccinated from the first study.

4. Randomization

Describe how samples/organisms/participants were allocated into experimental groups.

Monkeys were arbitrarily (non-randomly) assigned to treatments, and were randomly assigned order of elective necropsy.

5. Blinding

Describe whether the investigators were blinded to group allocation during data collection and/or analysis.

Veterinarians were blinded when evaluating CT scans, but not otherwise.

Note: all in vivo studies must report how sample size was determined and whether blinding and randomization were used.

6. Statistical parameters

For all figures and tables that use statistical methods, confirm that the following items are present in relevant figure legends (or in the Methods section if additional space is needed).

- | n/a | Confirmed |
|--------------------------|--|
| <input type="checkbox"/> | <input checked="" type="checkbox"/> The <u>exact sample size</u> (<i>n</i>) for each experimental group/condition, given as a discrete number and unit of measurement (animals, litters, cultures, etc.) |
| <input type="checkbox"/> | <input checked="" type="checkbox"/> A description of how samples were collected, noting whether measurements were taken from distinct samples or whether the same sample was measured repeatedly |
| <input type="checkbox"/> | <input checked="" type="checkbox"/> A statement indicating how many times each experiment was replicated |
| <input type="checkbox"/> | <input checked="" type="checkbox"/> The statistical test(s) used and whether they are one- or two-sided <i>Only common tests should be described solely by name; describe more complex techniques in the Methods section.</i> |
| <input type="checkbox"/> | <input checked="" type="checkbox"/> A description of any assumptions or corrections, such as an adjustment for multiple comparisons |
| <input type="checkbox"/> | <input checked="" type="checkbox"/> Test values indicating whether an effect is present <i>Provide confidence intervals or give results of significance tests (e.g. P values) as exact values whenever appropriate and with effect sizes noted.</i> |
| <input type="checkbox"/> | <input checked="" type="checkbox"/> A clear description of statistics including <u>central tendency</u> (e.g. median, mean) and <u>variation</u> (e.g. standard deviation, interquartile range) |
| <input type="checkbox"/> | <input checked="" type="checkbox"/> Clearly defined error bars in <u>all</u> relevant figure captions (with explicit mention of central tendency and variation) |

See the web collection on [statistics for biologists](#) for further resources and guidance.

► Software

Policy information about [availability of computer code](#)

7. Software

Describe the software used to analyze the data in this study.

R version 3.3.2 and several R packages as referenced in the Methods (up-to-date versions as of July 2017). Processed RNA-Seq read pairs were aligned using STAR (v.2.3.0.1). Read pairs in which both ends mapped concordantly were used as input to the HTseq Python program to assign gene counts. Flow cytometry data collected using BD FACSDiva v8.01 (Becton Dickinson) and analyzed using FloJo v9.9 (FlowJo LLC). Graphs generated using Prism 6 for Mac OSX (GraphPad Software, Inc).

For manuscripts utilizing custom algorithms or software that are central to the paper but not yet described in the published literature, software must be made available to editors and reviewers upon request. We strongly encourage code deposition in a community repository (e.g. GitHub). *Nature Methods* [guidance for providing algorithms and software for publication](#) provides further information on this topic.

► Materials and reagents

Policy information about [availability of materials](#)

8. Materials availability

Indicate whether there are restrictions on availability of unique materials or if these materials are only available for distribution by a third party.

All unique materials are available from the authors.

9. Antibodies

Describe the antibodies used and how they were validated for use in the system under study (i.e. assay and species).

| Antibodies | Clone # | fluochrome | supplier | name | catalog # | Lot # | Note/comments |
|-------------|--------------------|--------------|------------------|----------------|-------------|-------|--|
| CD28 | CD28.2 | Pure | Coul | IMBULK1 | 11EUR266 | | co-Stim |
| CD28 | CD28.2 | Pure | Ebio | 7014-0289-M050 | E10361-1632 | | |
| CD28 | CD28.2 | Pure | Affymetrix | CUST03277 | C10692 | | |
| CD49d | 9F10 | Pure | Ebio | 7014-0499-M050 | E10421-1632 | | co-stim CD49d 9F10 Pure Affymetrix CUST03278 C10693 |
| CD3 | SP34-2 | Pacific Blue | BD Bioscience | 624034 | 33062 | | Stim |
| CD3 | SP34-2 | Pacific Blue | BD Bioscience | 624034 | 3121927 | | Stim |
| CD3 | SP34-2 | Pacific Blue | BD Bioscience | 624034 | 4086967 | | Stim |
| CD3 | SP34-2 | Pacific Blue | BD Bioscience | 624034 | 4315653 | | Stim |
| CD3 | SP34-2 | Pacific Blue | BD Bioscience | 624034 | 5217827 | | Stim |
| CD3 | SP34-2 | Pacific Blue | BD Bioscience | 624034 | 6102907 | | Stim |
| CD3 | SP34-2 | Alexa700 | BD Bioscience | 624042 | 3214650 | | Stim |
| CD3 | SP34-2 | PerCP-Cy5.5 | BD Bioscience | 624060 | | | Phenotype |
| CD8a | SK-1 | PerCP-Cy5.5 | eBio | 7046-0087-M010 | E12102-1418 | | Stim |
| CD8 | RPA-T8 | APC | Affymetrix | 7017-0088-M002 | E15761-102 | | Phenotype |
| CD8 | RPA-T8 | APC | Affymetrix | CUST02887 | C10187 | | Phenotype |
| CD8 | RPA-T8 | APC | Affymetrix | 301014 | B145083 | | Phenotype |
| TNFa | MAB11 | FITC | BD Bioscience | 624045 | 2317639 | | ICS/Phenotype |
| TNFa | MAB11 | FITC | eBio | CUST03355 | C10685 | | ICS/Phenotype |
| TNFa | MAB11 | FITC | BD Bioscience | 624046 | 4325504 | | ICS/Phenotype |
| TNFa | MAB11 | FITC | Affymetrix | CUST03355 | C10685 | | ICS/Phenotype |
| TNFa | MAB11 | PE | BD Bioscience | 624049 | 4325520 | | Stim |
| TNFa | MAB11 | PE | Affymetrix | CUST03626 | C10636 | | Stim |
| IFNg | B27 | APC | BD Bioscience | 624078 | 2282636 | | Stim |
| IFNg | B27 | APC | BD Bioscience | 624078 | 4325543 | | Stim |
| IFNg | B27 | APC | BD Bioscience | 624078 | 6321681 | | Stim |
| CD69 | FN50 | PE | Affymetrix | CUST01282 | E20639-101 | | Stim/Phenotype |
| CD69 | FN50 | PE-TexasRed | BD Bioscience | 624005 | 04878 | | Stim |
| CD69 | FN50 | PE-TexasRed | BD Bioscience | 624005 | 01472 | | Stim |
| CD69 | FN50 | PE-TexasRed | BD Bioscience | 624005 | 3050570 | | Stim |
| CD69 | FN50 | PE-TexasRed | BD Bioscience | 624005 | 4161876 | | Stim |
| Ki-67 | B56 | FITC | BD Bioscience | 624046 | 2167972 | | Stim/Phenotype |
| Ki-67 | B56 | FITC | BD Bioscience | 624046 | 4086952 | | Stim/Phenotype |
| Ki-67 | B56 | FITC | BD Bioscience | 624046 | 6018769 | | Stim/Phenotype |
| CD28 | CD28.2 | PE-TexasRed | BD Bioscience | 624005 | 21562 | | Phenotype |
| CD28 | CD28.2 | PE-TexasRed | BD Bioscience | 624005 | 42785 | | Phenotype |
| CD95 | DX2 | PE | Affymetrix | CUST00525 | E18811-101 | | Phenotype |
| CD95 | DX2 | PE | BD Bioscience | 94203 | B237096 | | Phenotype |
| CCR7 | 15053 | Pacific Blue | Molecular Probes | C29272 | 86810A | | Phenotype |
| IL-2 | MQ1-17H12 | PE | BioLegend | 503808 | | | NA Stim |
| IL-2 | MQ1-17H12 | PE | Cy-7 | BioLegend | 503832 | | NA Stim |
| CD4 | L200 | AmCyan | BD Bioscience | 33917 | | | NA Stim |
| anti-MHC-I | mAb W6/32 | | BioLegend | 311402 | | | NA blocking |
| anti-MHC-II | mAb G46-6 (HLA-DR) | | BD Bioscience | 556642 | | | NA blocking Antibodies extensively validated in house by staining pattern and/or functional assays in previously published work (see references 23-26, and34). |

10. Eukaryotic cell lines

a. State the source of each eukaryotic cell line used.

Rhesus Telomerized Fibroblasts and Primary Rhesus Fibroblasts were used for RhCMV-vector production. These cell lines, derived from ONPRC rhesus macaques, were established by the authors and validated by their ability to produce high titre RhCMV.

b. Describe the method of cell line authentication used.

Non-transformed primary cell lines were confirmed by cell morphology and ability to propagate RhCMV.

c. Report whether the cell lines were tested for mycoplasma contamination.

Fibroblast cell lines were mycoplasma free as determined by PCR using the Lookout (Mycoplasma PCR Detection Kit, Sigma cat# MP0035-1KT). Prior to virus production every starter is screened for mycoplasma contamination, cell lines are tested every 3 months.

d. If any of the cell lines used are listed in the database of commonly misidentified cell lines maintained by [ICLAC](#), provide a scientific rationale for their use.

No commonly misidentified cell lines were used.

► Animals and human research participants

Policy information about [studies involving animals](#); when reporting animal research, follow the [ARRIVE guidelines](#)

11. Description of research animals

Provide all relevant details on animals and/or animal-derived materials used in the study.

All animals used in this study were 3-6 year old Rhesus Macaques (*macaca mulata*) males of India origin.

Policy information about [studies involving human research participants](#)

12. Description of human research participants

Describe the covariate-relevant population characteristics of the human research participants.

Not applicable. No human subjects were used.